

# Electronic Supplementary Info

## **Mono-, di- and tetra- rhenium Fischer carbene complexes with thienothiophene substituents**

Zandria Lamprecht,<sup>a</sup> Shankara Radhakrishnan,<sup>a</sup> Alexander Hildebrandt,<sup>b</sup> Heinrich Lang,<sup>b</sup> David C. Liles,<sup>a</sup> Norann Weststrate,<sup>a</sup> and Simon Lotz<sup>a</sup> and Daniela I. Bezuidenhout,<sup>a,c\*</sup>

<sup>a</sup> *Department of Chemistry, University of Pretoria, Private Bag X20, Hatfield 0028, Pretoria, South Africa.*

<sup>b</sup> *Technische Universität Chemnitz, Fakultät für Naturwissenschaften, Institut für Chemie, Anorganische Chemie, D-09107 Chemnitz, Germany.*

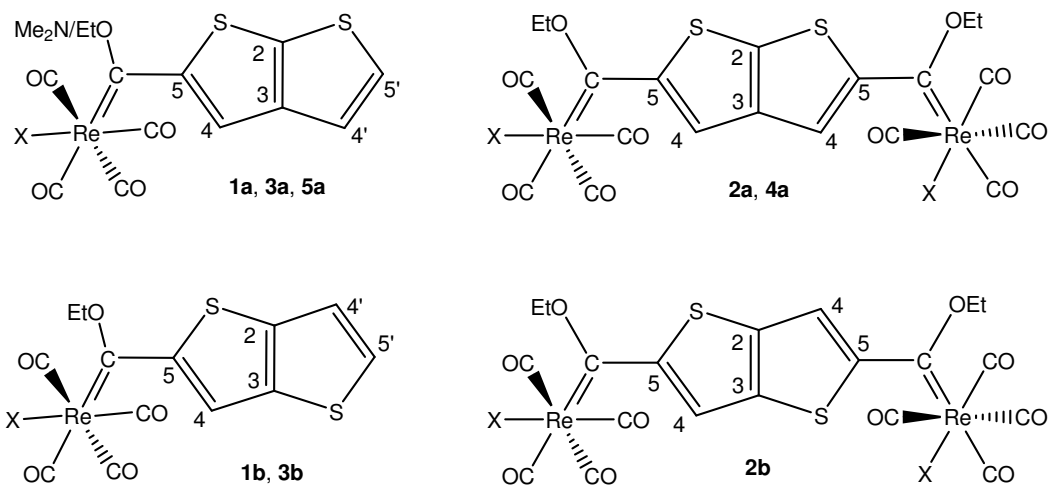
<sup>c</sup> *Molecular Sciences Institute, School of Chemistry, University of the Witwatersrand, Johannesburg 2050, South Africa.*

## Contents:

Figure S1: Atom numbering scheme used in NMR spectral assignment. ....	S4
Figure S2: $^1\text{H}$ NMR spectrum of <b>1a</b> in $\text{CDCl}_3$ . ....	S5
Figure S3: $^{13}\text{C}$ NMR spectrum of <b>1a</b> in $\text{CDCl}_3$ . ....	S5
Figure S4: 2D [ $^1\text{H}$ , $^{13}\text{C}$ ] HSQC NMR spectrum of <b>1a</b> in $\text{CDCl}_3$ . ....	S6
Figure S5: $^1\text{H}$ NMR spectrum of <b>2a</b> in $\text{CDCl}_3$ . ....	S6
Figure S6: $^{13}\text{C}$ NMR spectrum of <b>2a</b> in $\text{CDCl}_3$ . ....	S7
Figure S7: $^1\text{H}$ NMR spectrum of <b>3a</b> in $\text{CDCl}_3$ . ....	S7
Figure S8: $^{13}\text{C}$ NMR spectrum of <b>3a</b> in $\text{CDCl}_3$ . ....	S8
Figure S9: 2D [ $^1\text{H}$ , $^{13}\text{C}$ ] HSQC NMR spectrum of <b>3a</b> in $\text{CDCl}_3$ . ....	S8
Figure S10: $^1\text{H}$ NMR spectrum of <b>4a</b> in $\text{CDCl}_3$ . ....	S9
Figure S11: $^{13}\text{C}$ NMR spectrum of <b>4a</b> in $\text{CDCl}_3$ . ....	S9
Figure S12: $^1\text{H}$ NMR spectrum of <b>5a</b> in $\text{CDCl}_3$ . ....	S10
Figure S13: $^{13}\text{C}$ NMR spectrum of <b>5a</b> in $\text{CDCl}_3$ . ....	S10
Figure S14: 2D [ $^1\text{H}$ , $^{13}\text{C}$ ] HSQC NMR spectrum of <b>5a</b> in $\text{CDCl}_3$ . ....	S11
Figure S15: $^1\text{H}$ NMR spectrum of <b>1b</b> in $\text{CDCl}_3$ . ....	S11
Figure S16: $^{13}\text{C}$ NMR spectrum of <b>1b</b> in $\text{CDCl}_3$ . ....	S12
Figure S17: 2D [ $^1\text{H}$ , $^{13}\text{C}$ ] HSQC NMR spectrum of <b>1b</b> in $\text{CDCl}_3$ . ....	S12
Figure S18: $^1\text{H}$ NMR spectrum of <b>3b</b> in $\text{CDCl}_3$ . ....	S13
Figure S19: $^{13}\text{C}$ NMR spectrum of <b>3b</b> in $\text{CDCl}_3$ . ....	S13
Figure S20: 2D [ $^1\text{H}$ , $^{13}\text{C}$ ] HSQC NMR spectrum of <b>3b</b> in $\text{CDCl}_3$ . ....	S14
Figure S21: Cyclic voltammograms of <b>1a</b> at positive potentials (red) and negative potentials (blue), at a glassy carbon electrode, scan rate $0.1 \text{ Vs}^{-1}$ in $\text{CH}_2\text{Cl}_2$ with the internal standard marked as FcH. ....	S15
Figure S22: Cyclic voltammograms of <b>2a</b> at positive potentials (red) and negative potentials (blue), at a glassy carbon electrode, scan rate $0.1 \text{ Vs}^{-1}$ in $\text{CH}_2\text{Cl}_2$ with the internal standard marked as FcH. ....	S15
Figure S23: Cyclic voltammograms of <b>3a</b> at positive potentials (red) and negative potentials (blue), at a glassy carbon electrode, scan rate $0.1 \text{ Vs}^{-1}$ in $\text{CH}_2\text{Cl}_2$ with the internal standard marked as FcH. ....	S15
Figure S24: Cyclic voltammograms of <b>5a</b> at positive potentials (red) and negative potentials (blue), at a glassy carbon electrode, scan rate $0.1 \text{ Vs}^{-1}$ in $\text{CH}_2\text{Cl}_2$ with the internal standard marked as FcH. ....	S16
Figure S25: Cyclic voltammograms of <b>1b</b> at positive potentials (red) and negative potentials (blue), at a glassy carbon electrode, scan rate $0.1 \text{ Vs}^{-1}$ in $\text{CH}_2\text{Cl}_2$ with the internal standard marked as FcH. ....	S16
Figure S26: Cyclic voltammograms of <b>3b</b> at positive potentials (red) and negative potentials (blue), at a glassy carbon electrode, scan rate $0.1 \text{ Vs}^{-1}$ in $\text{CH}_2\text{Cl}_2$ with the internal standard marked as FcH. ....	S16
Figure S27: SEC-IR of <b>1a</b> upon reduction. Red: neutral compound; blue: reduced compound. ....	S17
Figure S28: SEC-IR of <b>3a</b> upon reduction. Red: neutral compound; blue: reduced compound. ....	S17
Figure S29: Intramolecular and intermolecular interactions found in the crystal packing of <b>3a</b> and <b>3b</b> . ....	S18
Table S1: Crystal data and structure refinement for complexes <b>1a</b> , <b>2a</b> , <b>3a</b> , <b>5a</b> , <b>1b</b> and <b>3b</b> . ....	S19
Table S2: Chemical potential ( $\mu$ ), hardness/MO energy gap ( $\eta$ ) and electrophilicity index ( $\omega$ ) reported in eV for <b>1a</b> , <b>1b</b> , <b>3a</b> and <b>3b</b> . ....	S20
Table S3: Major experimental UV-Vis transitions their corresponding calculated molecular orbitals for <b>1a</b> . ....	S21
Figure S30: Normal Transition orbitals (NTOs) for the major absorption bands of <b>1a</b> . ....	S21
Figure S31: Normal Transition orbitals (NTOs) for the major absorption bands of <b>1a</b> $^-$ . ....	S22
Figure S32: Spin population of <b>1a</b> $^-$ and <b>1a</b> $^+$ on the left and right hand side respectively. ....	S22
Table S4: Major experimental UV-Vis transitions their corresponding calculated molecular orbitals for <b>1b</b> . ....	S23
Figure S33: Normal Transition orbitals (NTOs) for the major absorption bands of <b>1b</b> . ....	S23
Figure S34: Normal Transition orbitals (NTOs) for the major absorption bands of <b>1b</b> $^-$ . ....	S24
Figure S35: Spin population of <b>1b</b> $^-$ and <b>1b</b> $^+$ on the left and right hand side respectively. ....	S24
Figure S36: Changes in UV-Vis absorption spectrum of <b>2a</b> during the reduction event in $\text{CH}_2\text{Cl}_2$ containing $0.1 \text{ M}$ $\text{N}^n\text{Bu}_4[\text{B}(\text{C}_6\text{F}_5)_4]$ electrolyte, applied voltage range: $-1.1$ to $-1.4 \text{ V}$ ; The inset shows the appearance of a $1600 \text{ nm}$ Intervalence charge transfer (IVCT) feature at an applied voltage $-1.4 \text{ V}$ . (Legend: Increasing cathodic voltages from black to light green). ....	S25

Figure S37: Changes in UV-Vis absorption spectrum of **3a** during the reduction event in CH<sub>2</sub>Cl<sub>2</sub> containing 0.1 M N<sup>n</sup>Bu<sub>4</sub>[B(C<sub>6</sub>F<sub>5</sub>)<sub>4</sub>] electrolyte, applied voltage range: -1.1 to -1.4 V (Legend: Increasing cathodic voltages from black to light green)..... S25

Figure S38: Changes in UV-Vis absorption spectrum of **3b** during the reduction event in CH<sub>2</sub>Cl<sub>2</sub> containing 0.1 M N<sup>n</sup>Bu<sub>4</sub>[B(C<sub>6</sub>F<sub>5</sub>)<sub>4</sub>] electrolyte, applied voltage range: -1.1 to -1.4 V (Legend: Increasing cathodic voltages from black to light green)..... S26



X = Re(CO)<sub>5</sub>, Br, Cl

**Figure S1:** Atom numbering scheme used in NMR spectral assignment.

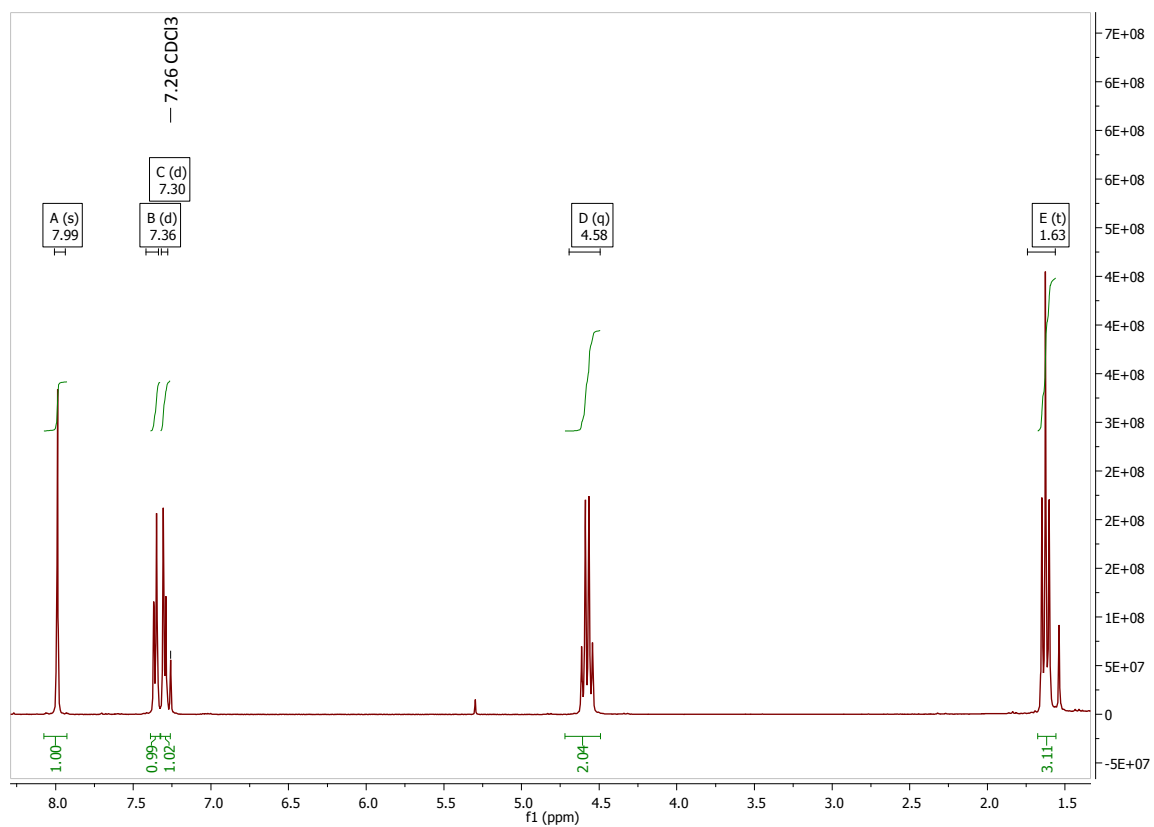


Figure S2:  $^1\text{H}$  NMR spectrum of **1a** in  $\text{CDCl}_3$ .

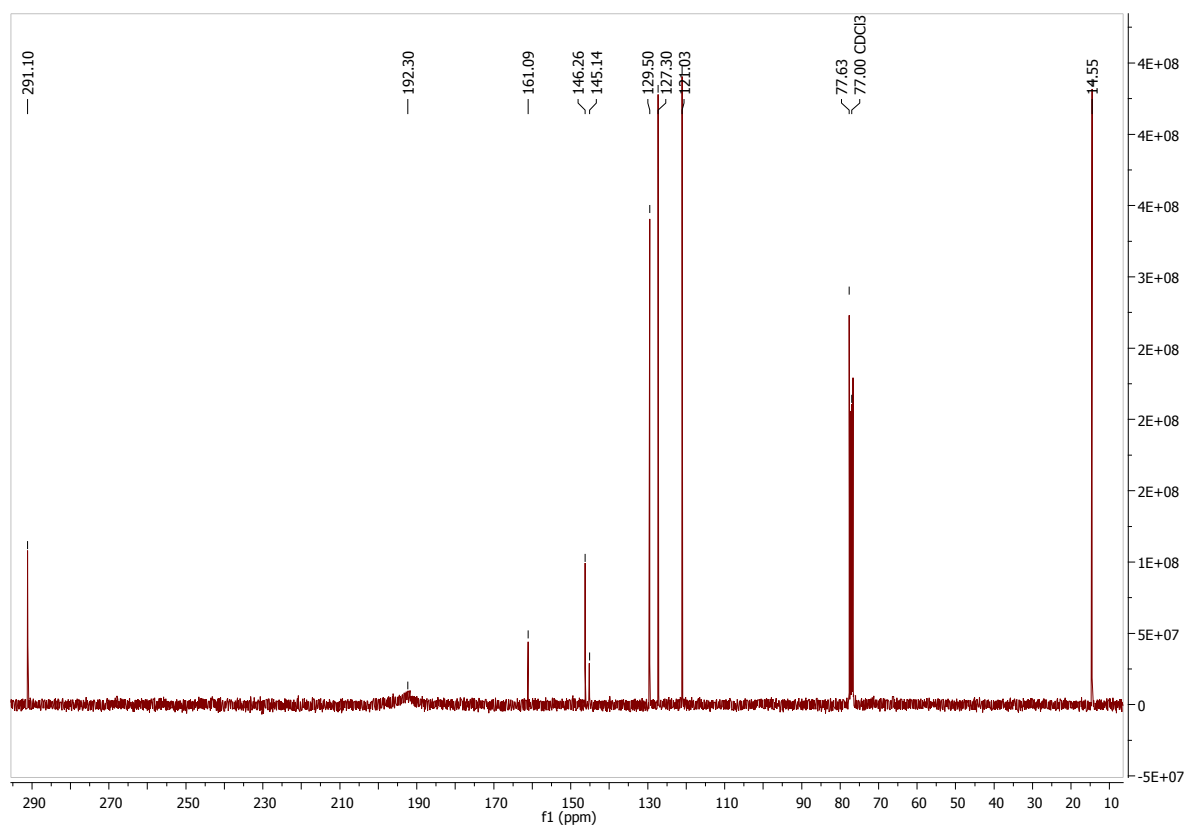


Figure S3:  $^{13}\text{C}$  NMR spectrum of **1a** in  $\text{CDCl}_3$ .

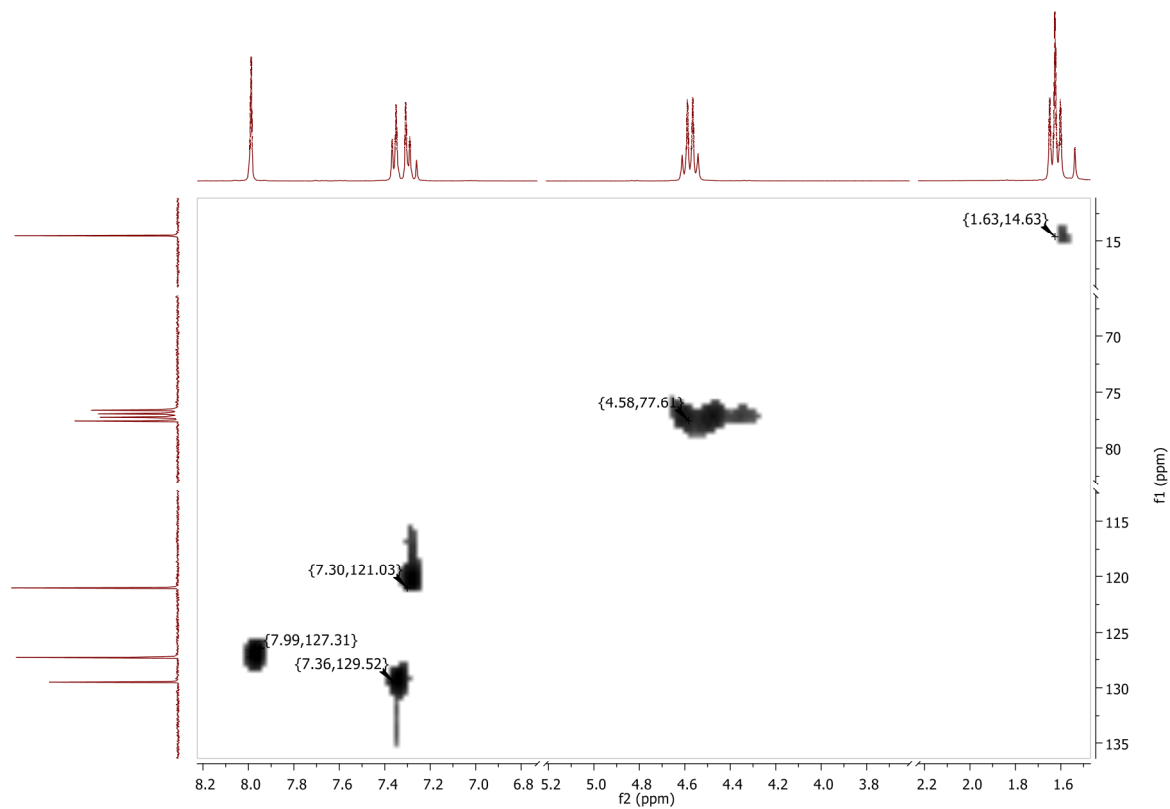


Figure S4: 2D  $^1\text{H}$ ,  $^{13}\text{C}$  HSQC NMR spectrum of **1a** in  $\text{CDCl}_3$ .

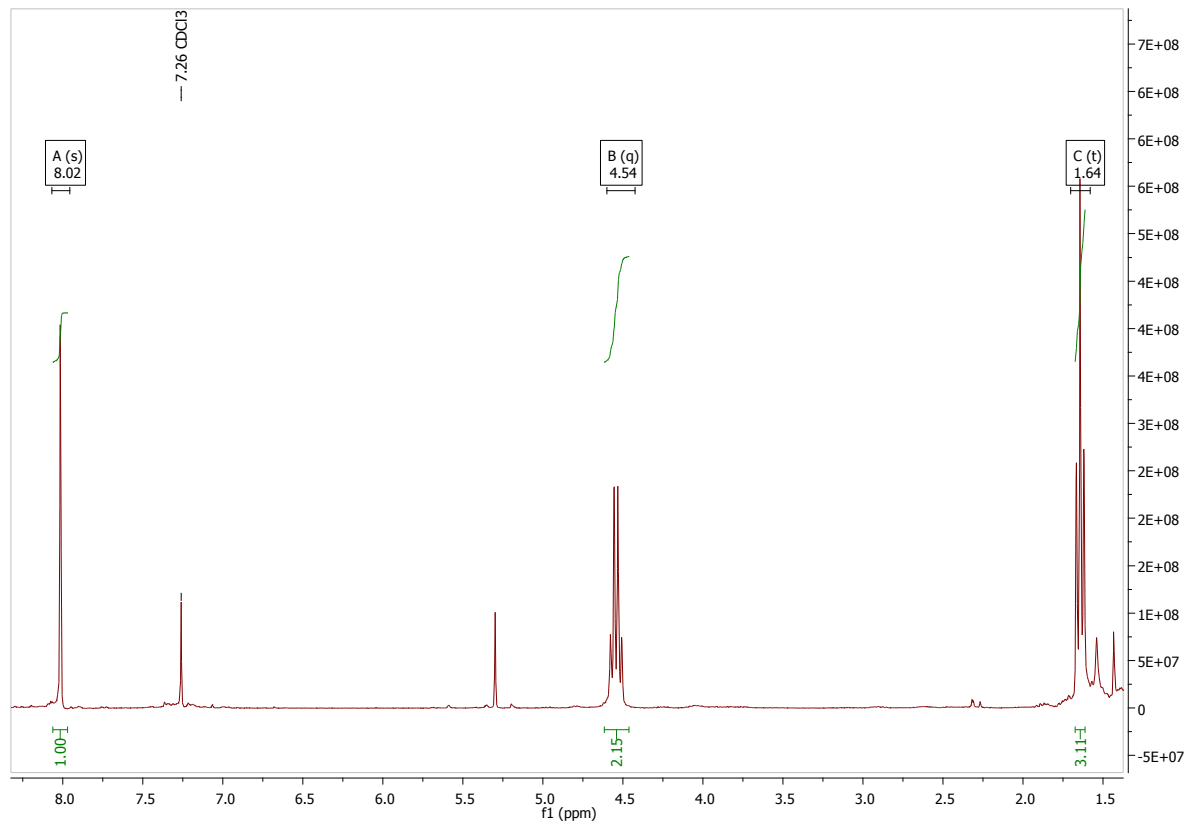


Figure S5:  $^1\text{H}$  NMR spectrum of **2a** in  $\text{CDCl}_3$ .

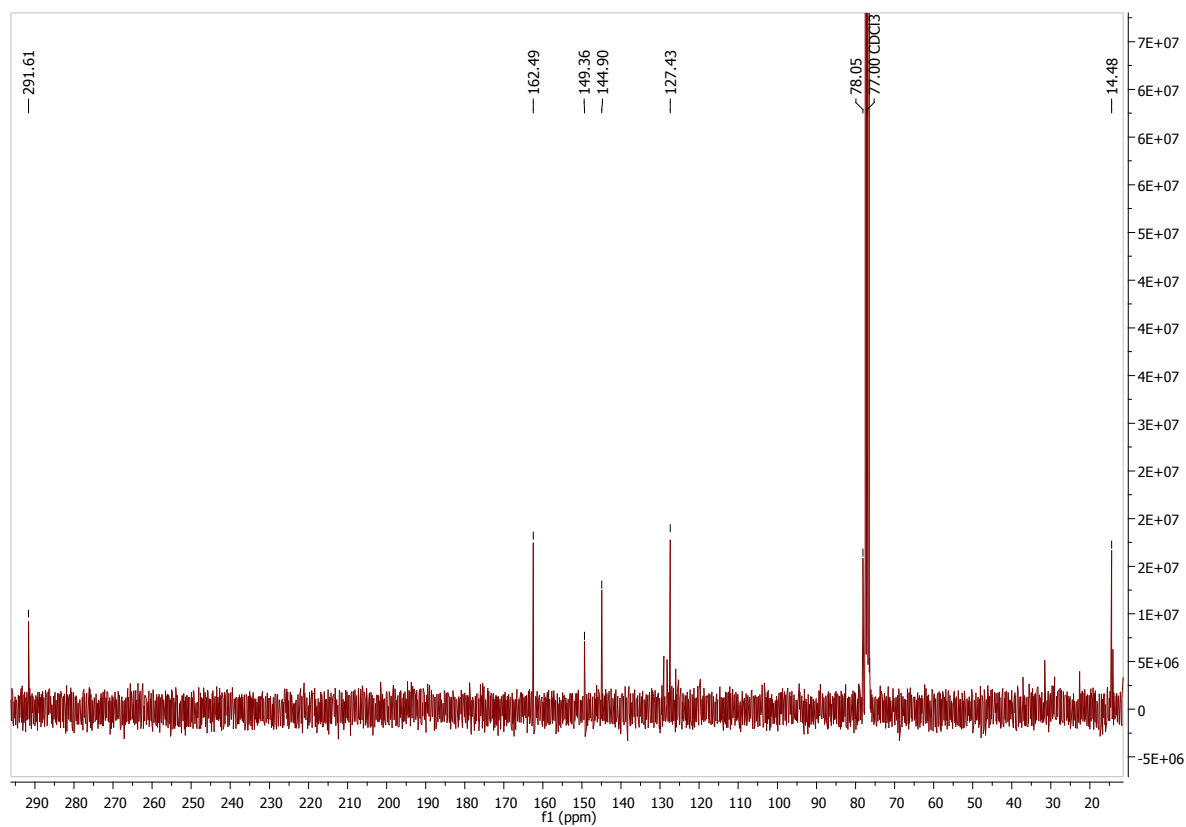


Figure S6:  $^{13}\text{C}$  NMR spectrum of **2a** in  $\text{CDCl}_3$ .

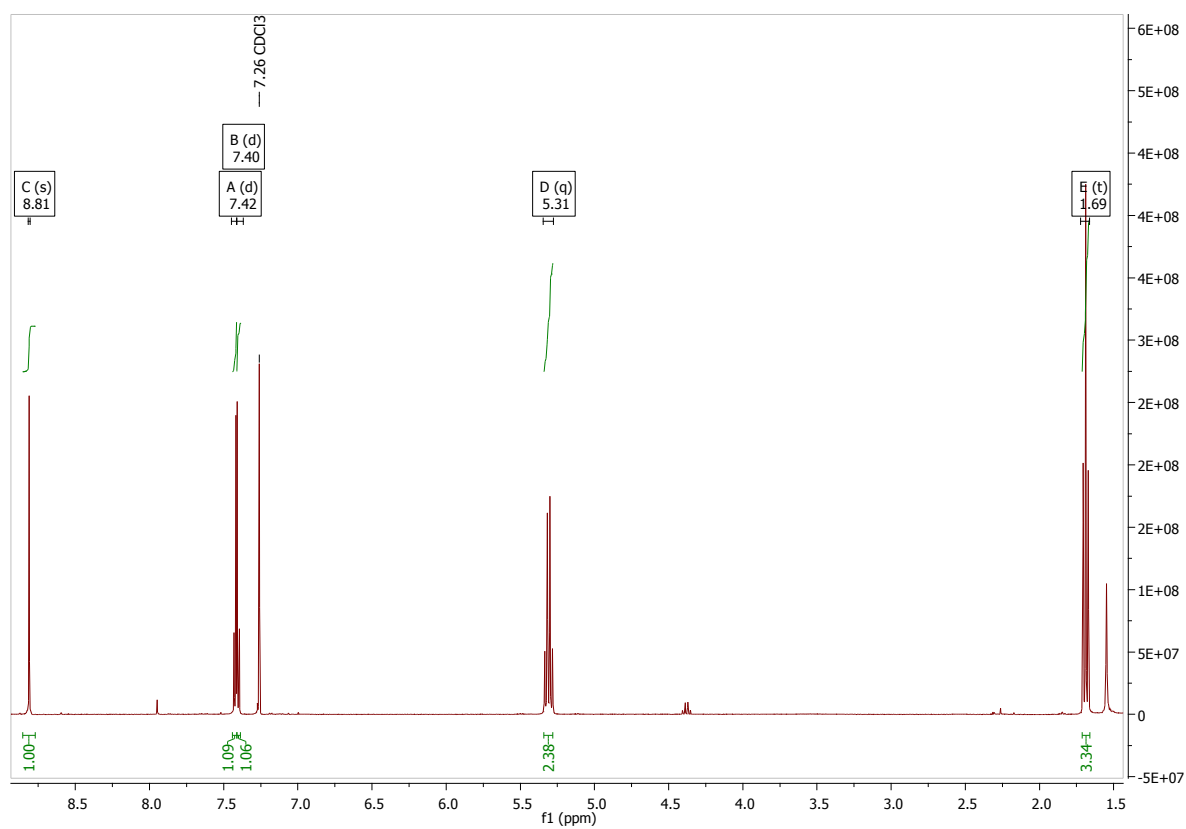


Figure S7:  $^1\text{H}$  NMR spectrum of **3a** in  $\text{CDCl}_3$ .

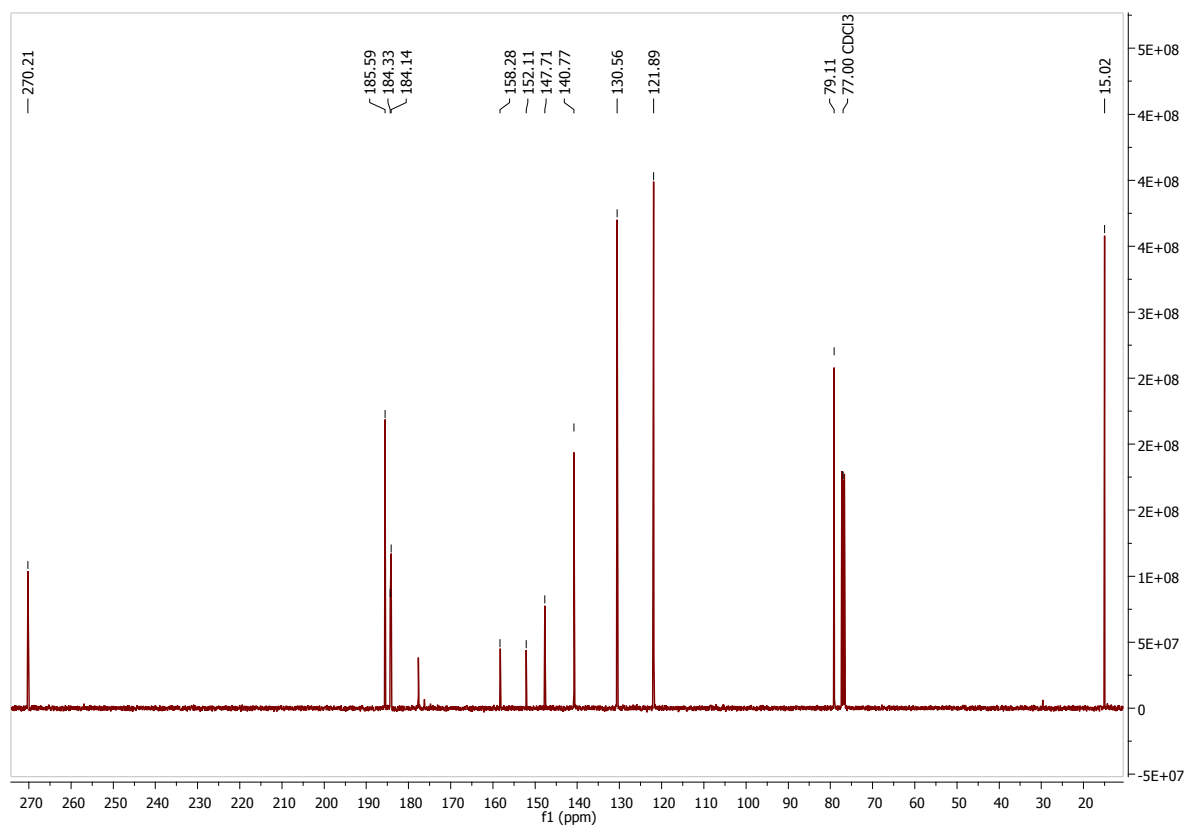


Figure S8:  $^{13}\text{C}$  NMR spectrum of **3a** in  $\text{CDCl}_3$ .

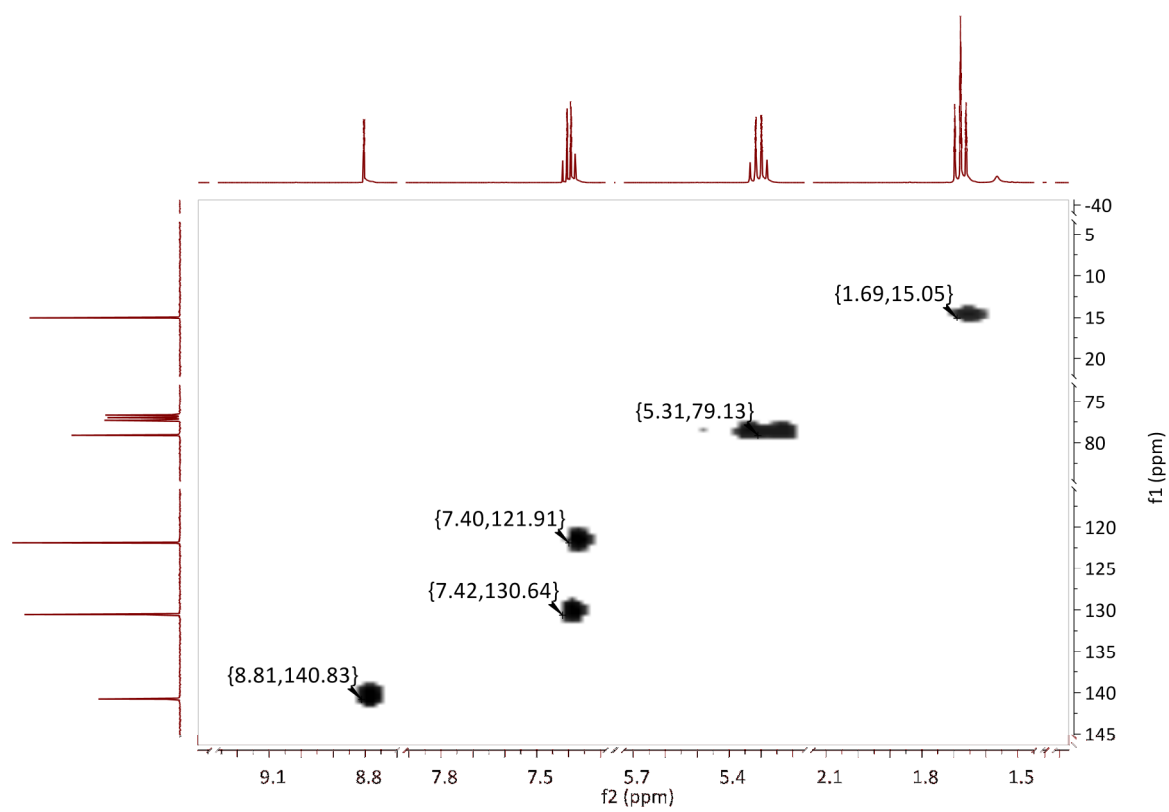


Figure S9: 2D  $^1\text{H}$ ,  $^{13}\text{C}$  HSQC NMR spectrum of **3a** in  $\text{CDCl}_3$ .



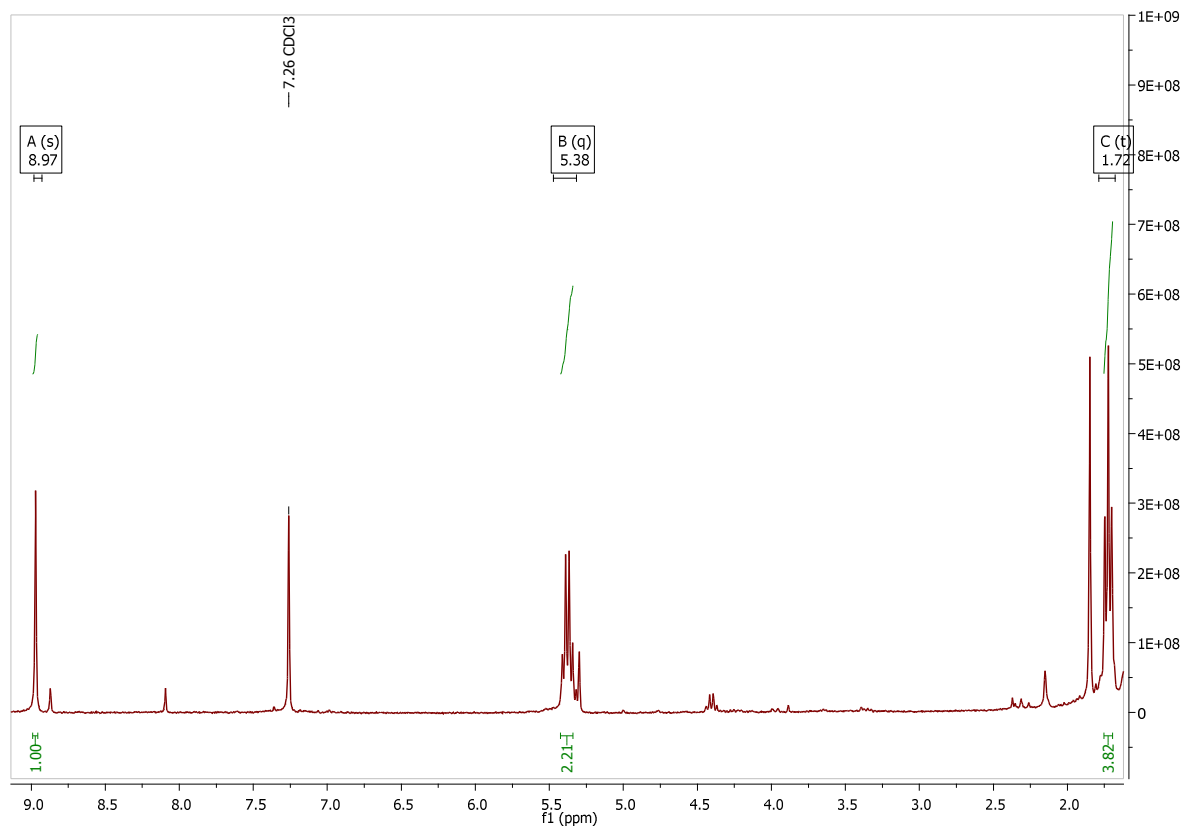


Figure S10:  $^1\text{H}$  NMR spectrum of **4a** in  $\text{CDCl}_3$ .

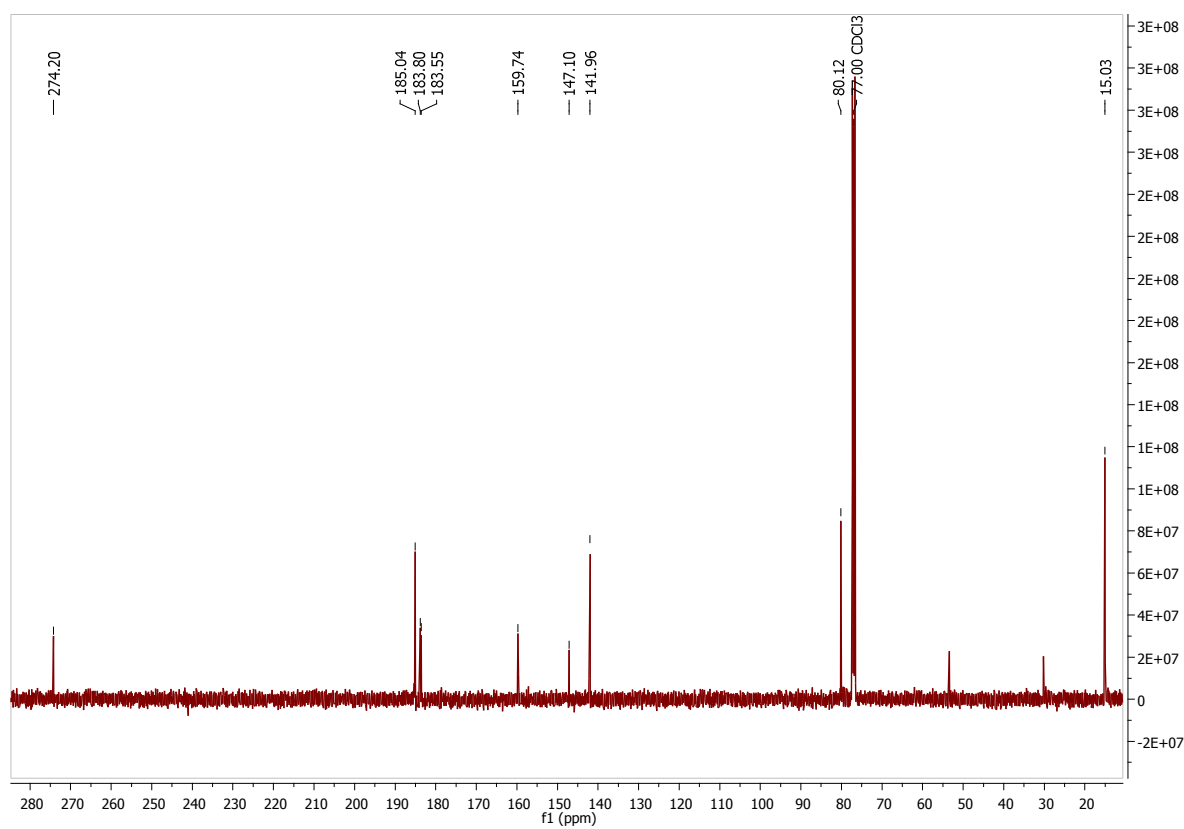


Figure S11:  $^{13}\text{C}$  NMR spectrum of **4a** in  $\text{CDCl}_3$ .

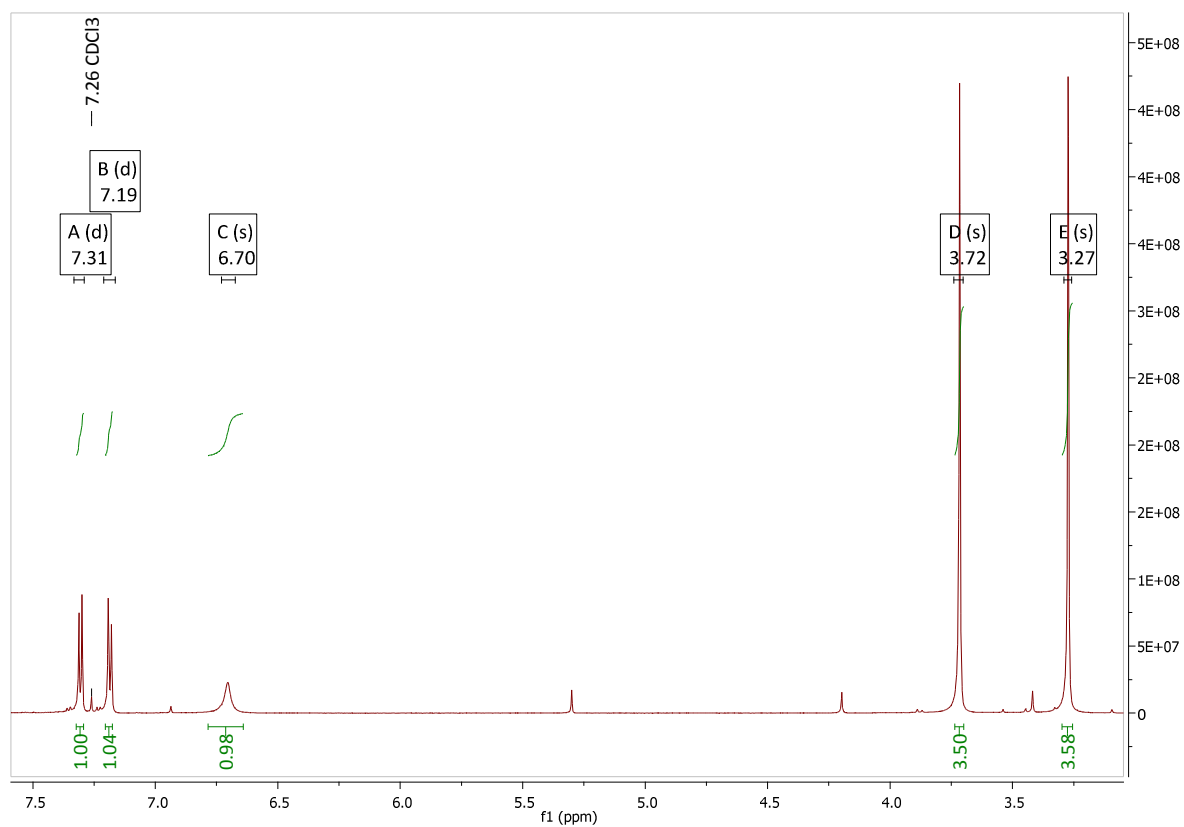


Figure S12:  $^1\text{H}$  NMR spectrum of **5a** in  $\text{CDCl}_3$ .

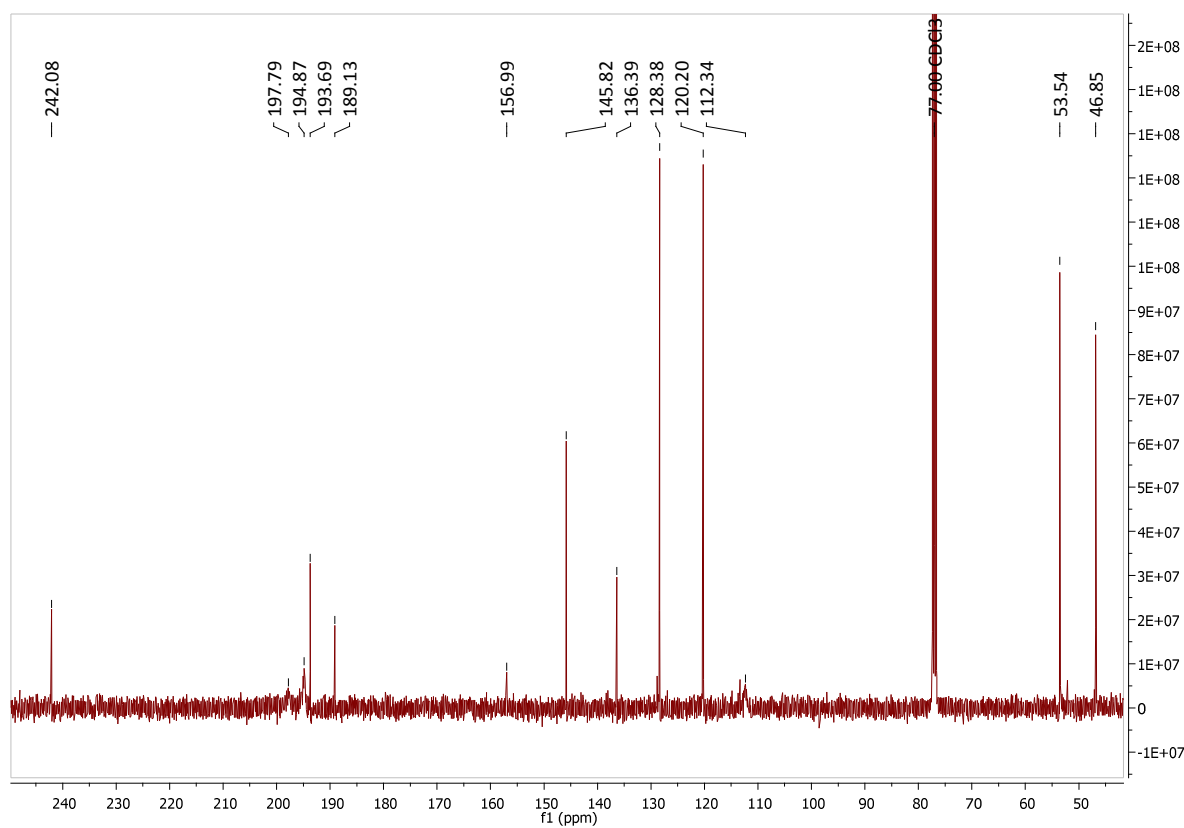


Figure S13:  $^{13}\text{C}$  NMR spectrum of **5a** in  $\text{CDCl}_3$ .

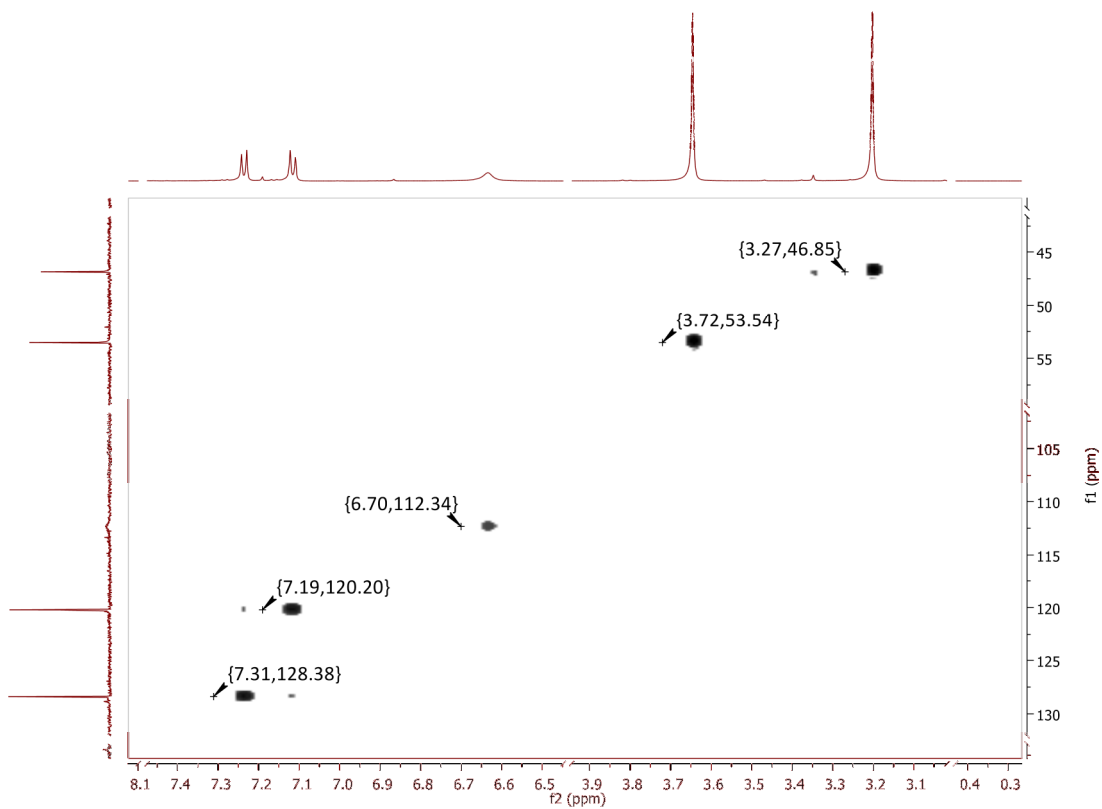


Figure S14: 2D [ $^1\text{H}$ ,  $^{13}\text{C}$ ] HSQC NMR spectrum of **5a** in  $\text{CDCl}_3$ .

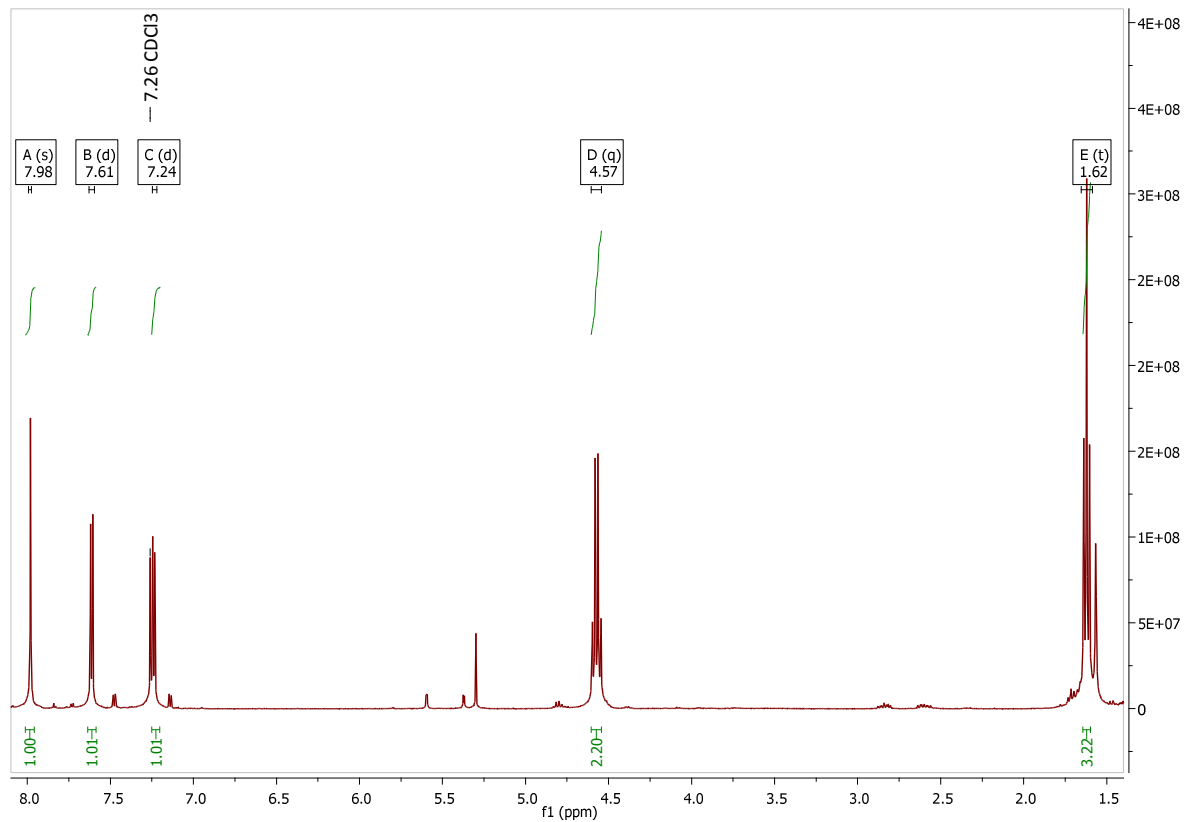


Figure S15:  $^1\text{H}$  NMR spectrum of **1b** in  $\text{CDCl}_3$ .

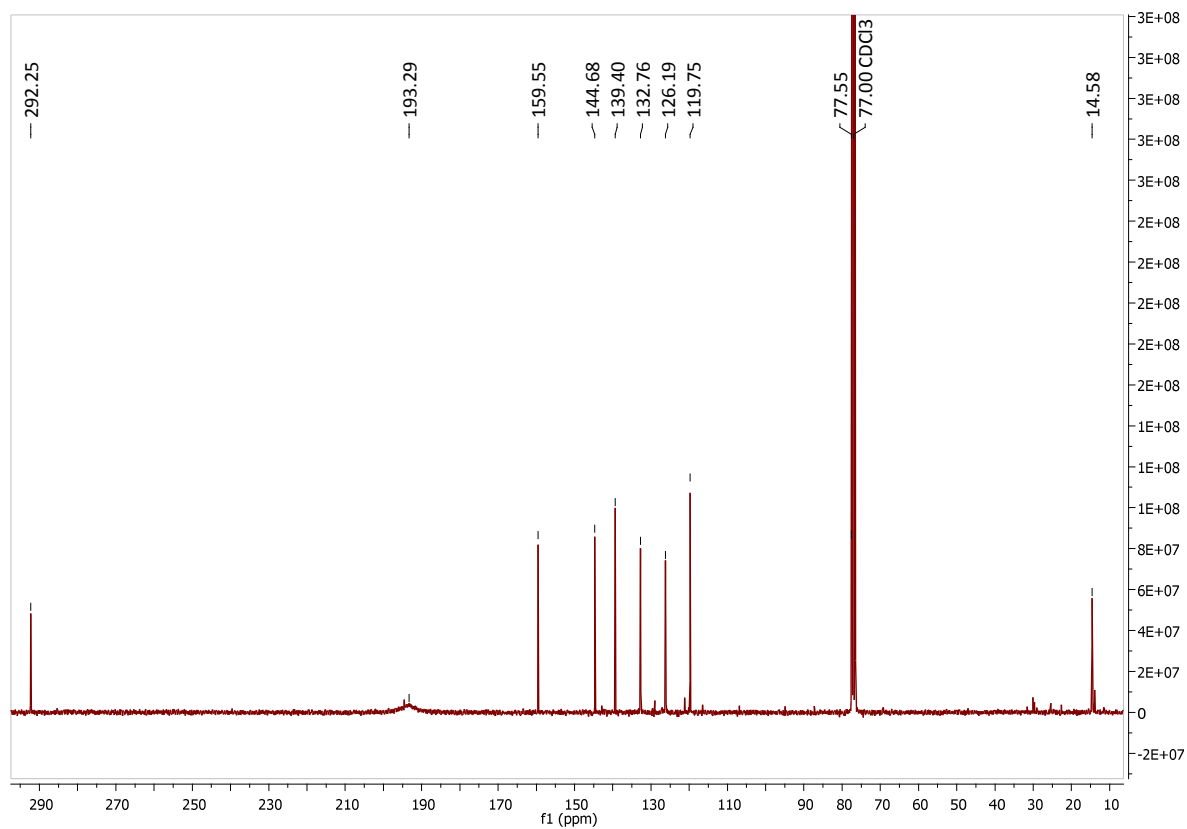


Figure S16:  $^{13}\text{C}$  NMR spectrum of **1b** in  $\text{CDCl}_3$ .

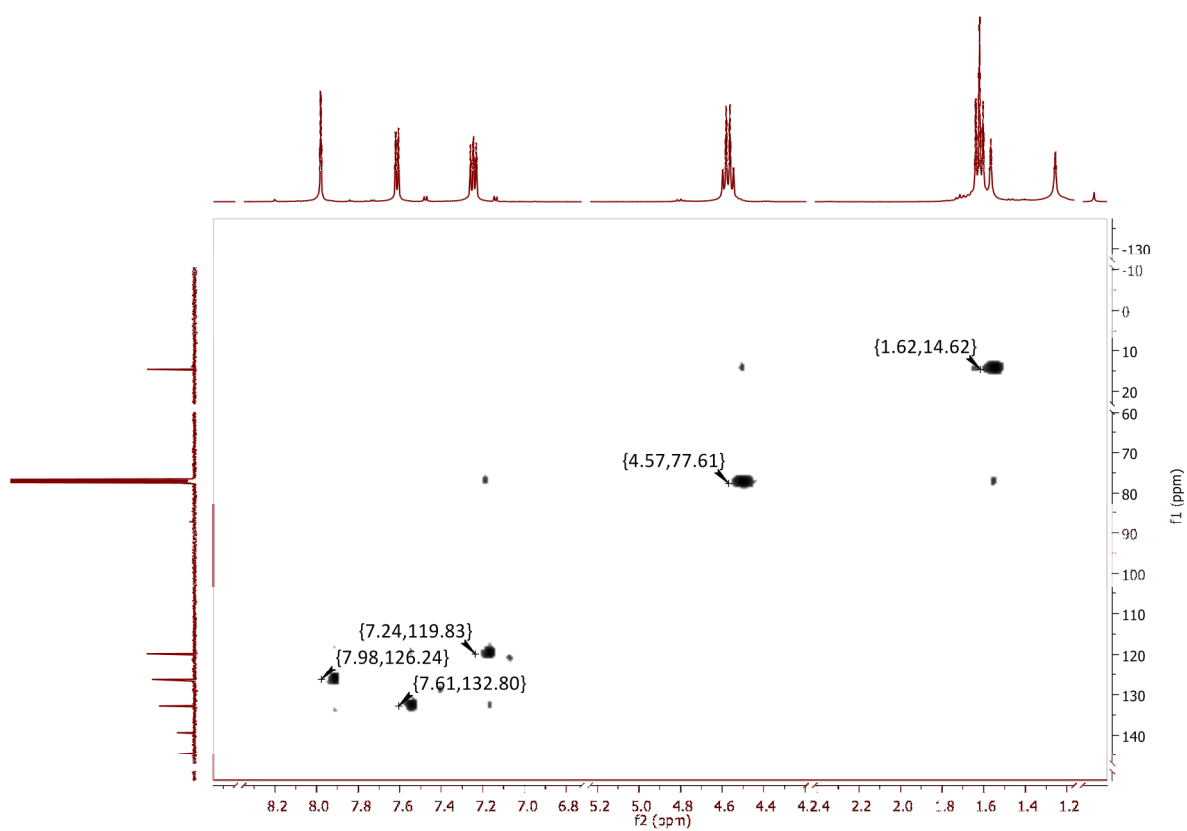


Figure S17: 2D  $[^1\text{H}, ^{13}\text{C}]$  HSQC NMR spectrum of **1b** in  $\text{CDCl}_3$ .

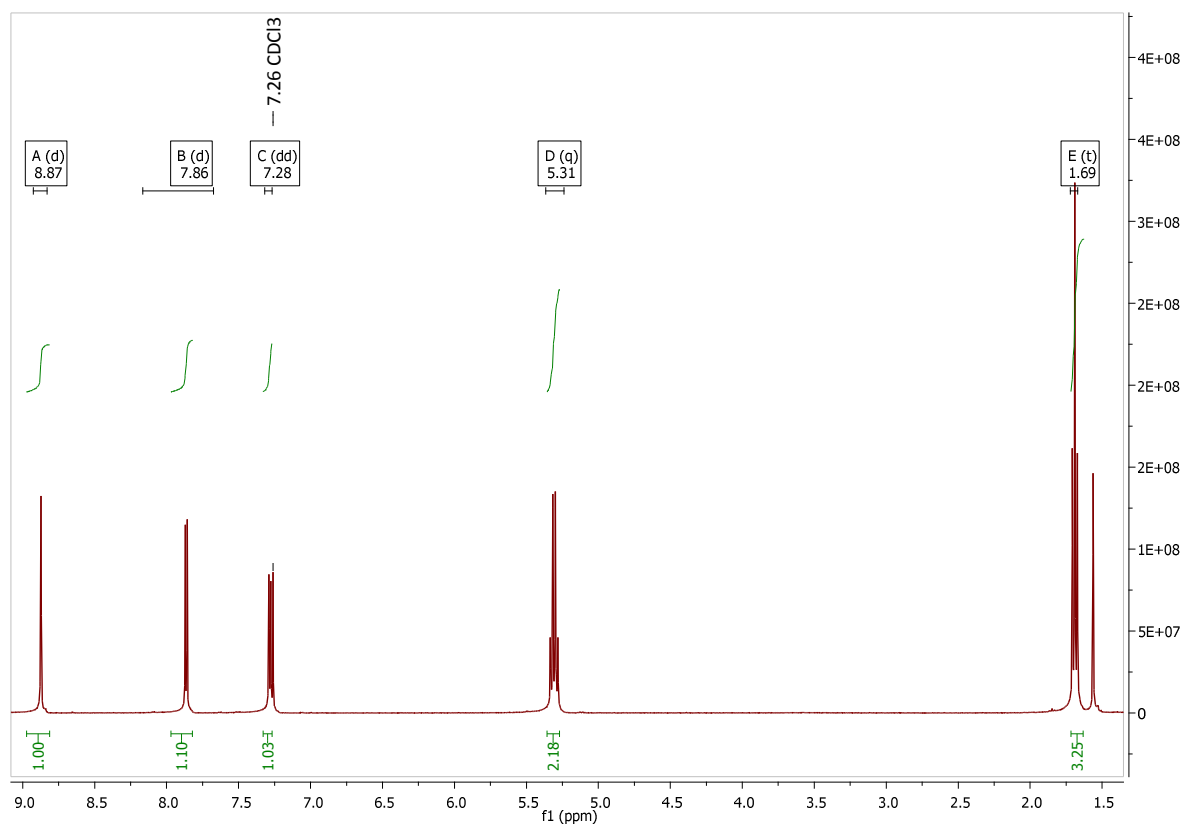


Figure S18:  $^1\text{H}$  NMR spectrum of **3b** in  $\text{CDCl}_3$ .

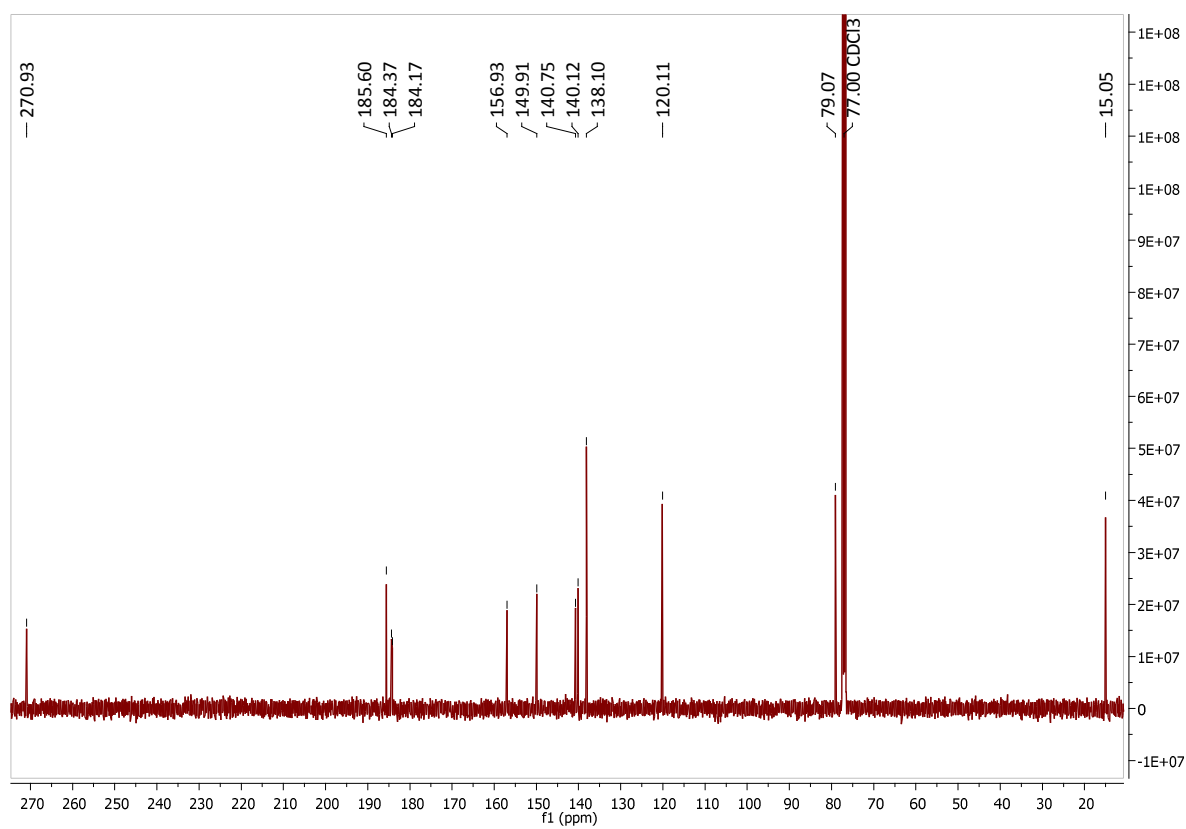


Figure S19:  $^{13}\text{C}$  NMR spectrum of **3b** in  $\text{CDCl}_3$ .

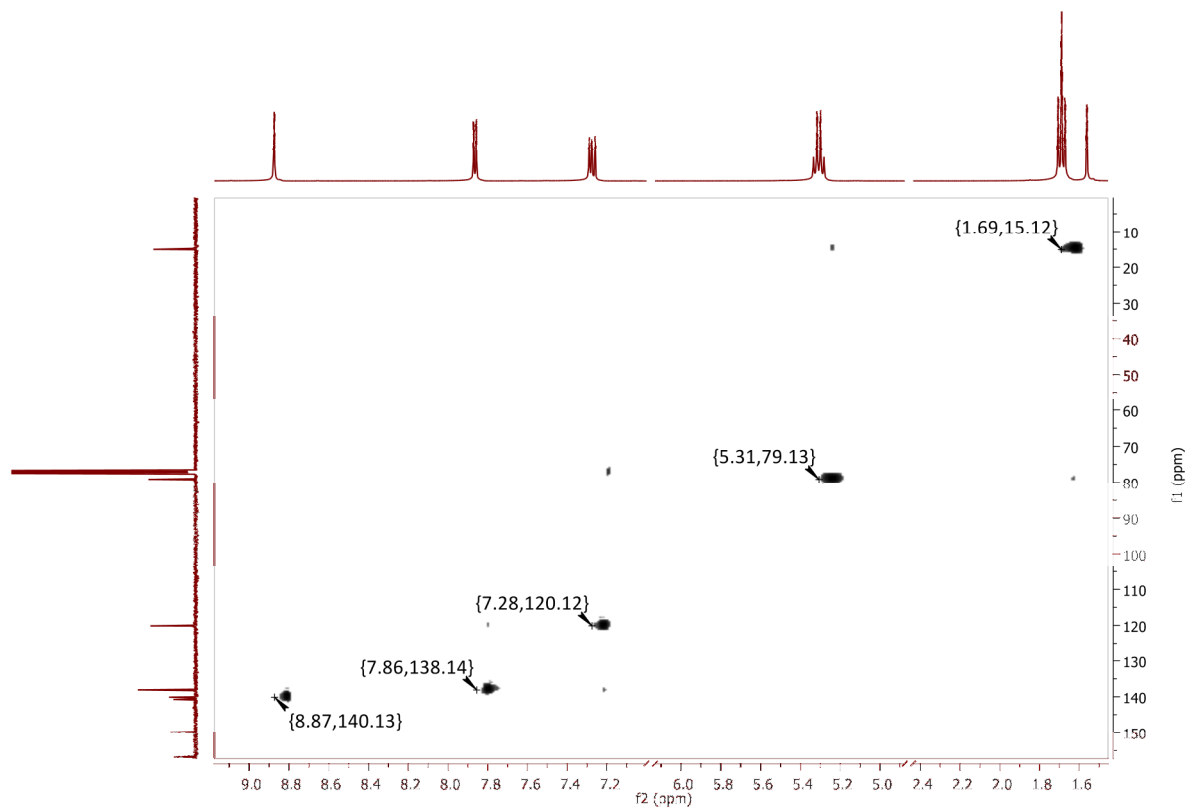
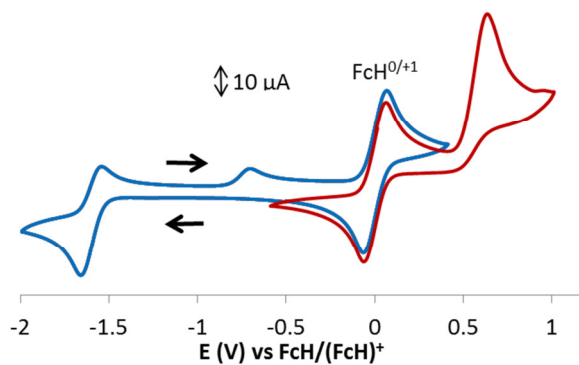
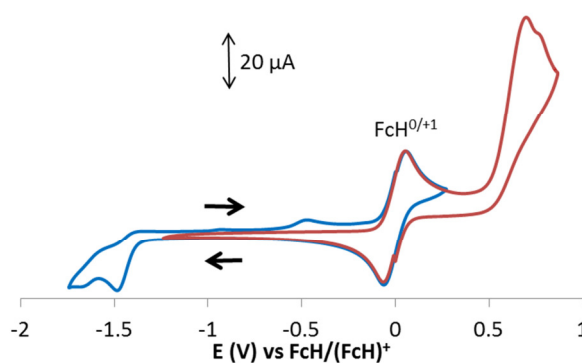


Figure S20: 2D [ $^1\text{H}$ ,  $^{13}\text{C}$ ] HSQC NMR spectrum of **3b** in  $\text{CDCl}_3$ .



**Figure S21:** Cyclic voltammograms of **1a** at positive potentials (red) and negative potentials (blue), at a glassy carbon electrode, scan rate  $0.1 \text{ Vs}^{-1}$  in  $\text{CH}_2\text{Cl}_2$  with the internal standard marked as FcH.



**Figure S22:** Cyclic voltammograms of **2a** at positive potentials (red) and negative potentials (blue), at a glassy carbon electrode, scan rate  $0.1 \text{ Vs}^{-1}$  in  $\text{CH}_2\text{Cl}_2$  with the internal standard marked as FcH.

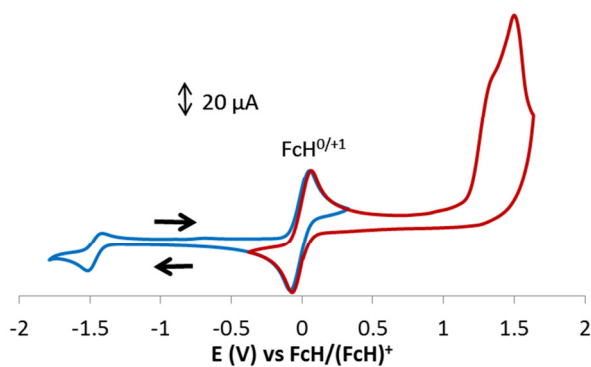


**Figure S23:** Cyclic voltammograms of **3a** at positive potentials (red) and negative potentials (blue), at a glassy carbon electrode, scan rate  $0.1 \text{ Vs}^{-1}$  in  $\text{CH}_2\text{Cl}_2$  with the internal standard marked as FcH.

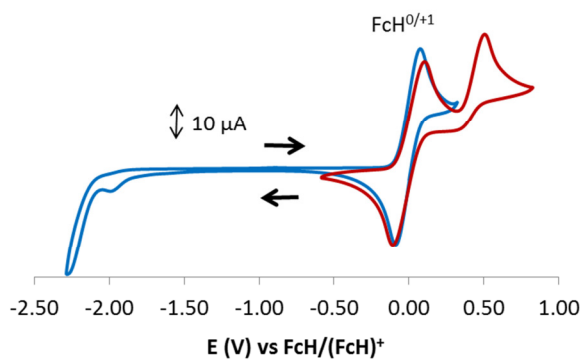


**Figure S24:** Cyclic voltammograms of **5a** at positive potentials (red) and negative potentials (blue), at a glassy carbon electrode, scan rate  $0.1 \text{ Vs}^{-1}$  in  $\text{CH}_2\text{Cl}_2$  with the internal standard marked as FcH.

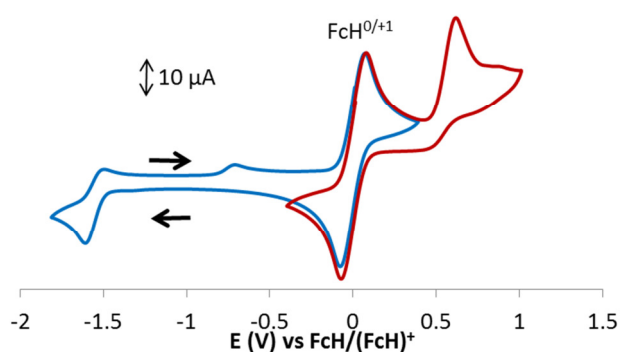


**Figure S25:** Cyclic voltammograms of **1b** at positive potentials (red) and negative potentials (blue), at a glassy carbon electrode, scan rate  $0.1 \text{ Vs}^{-1}$  in  $\text{CH}_2\text{Cl}_2$  with the internal standard marked as FcH.

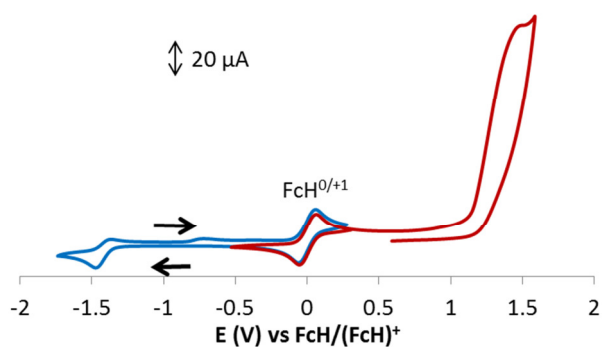


**Figure S26:** Cyclic voltammograms of **3b** at positive potentials (red) and negative potentials (blue), at a glassy carbon electrode, scan rate  $0.1 \text{ Vs}^{-1}$  in  $\text{CH}_2\text{Cl}_2$  with the internal standard marked as FcH.



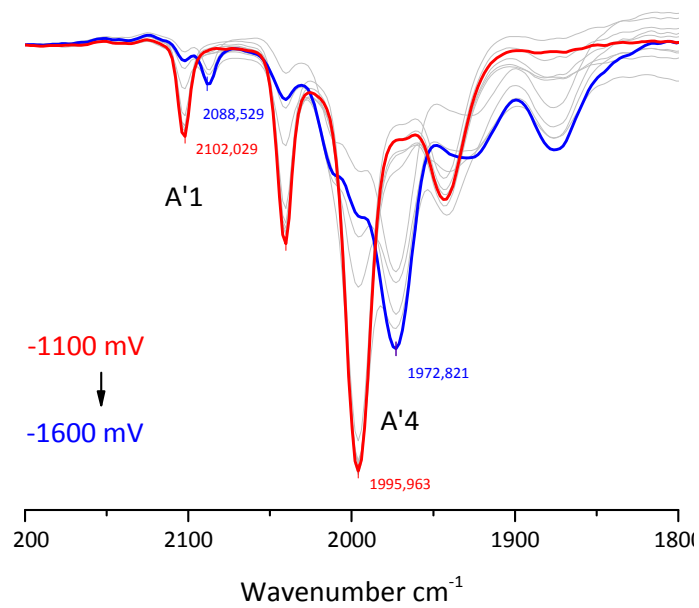


**Figure S27:** SEC-IR of **1a** upon reduction. Red: neutral compound; blue: reduced compound.

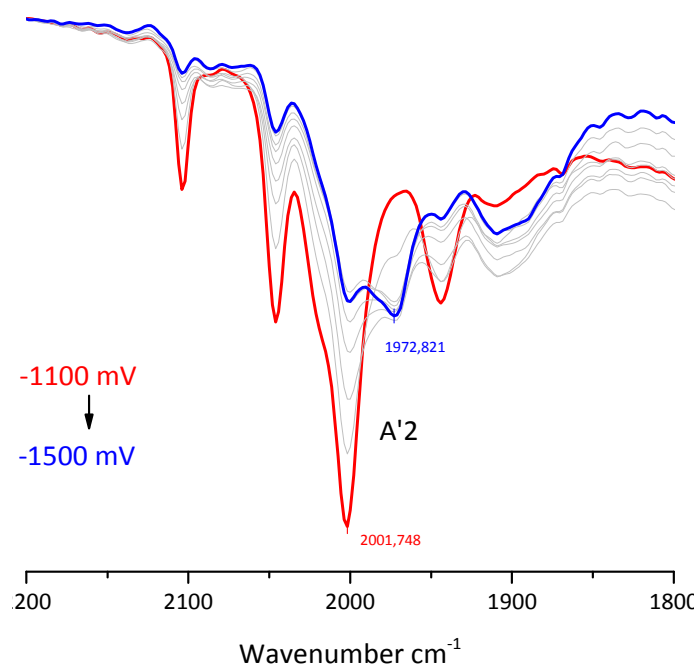


**Figure S28:** SEC-IR of **3a** upon reduction. Red: neutral compound; blue: reduced compound.

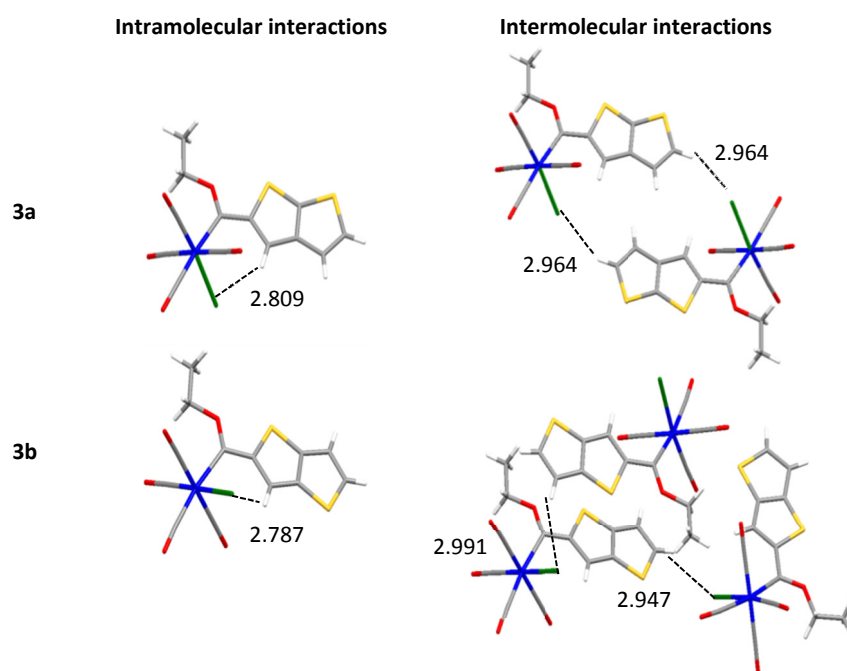


**Figure S29:** Intramolecular and intermolecular interactions found in the crystal packing of **3a** and **3b**.

**Table S1:** Crystal data and structure refinement for complexes **1a**, **2a**, **3a**, **5a**, **1b** and **3b**.

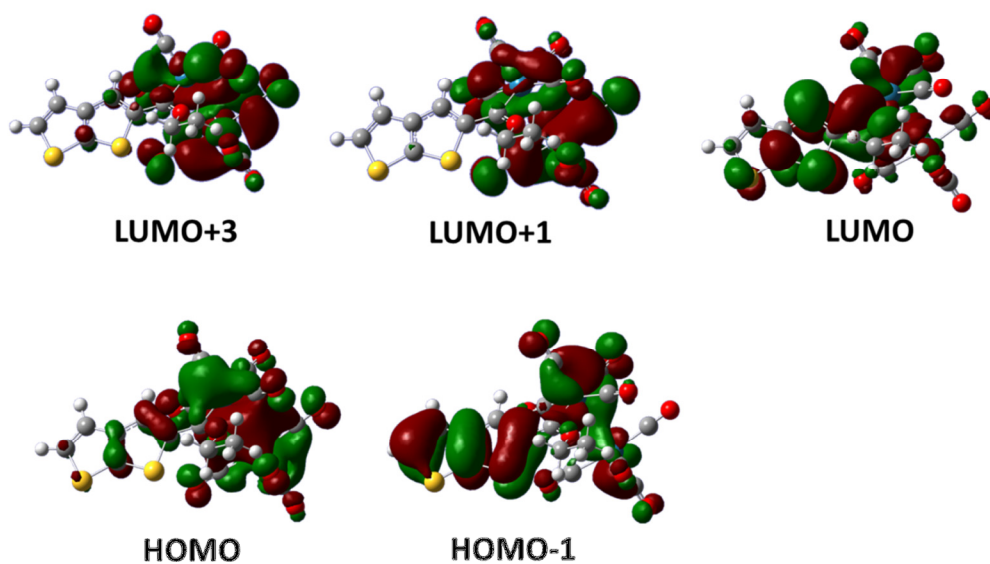
	<b>1a</b>	<b>2a</b>	<b>3a</b>	<b>5a</b>	<b>1b</b>	<b>3b</b>
Empirical formula	C <sub>18</sub> H <sub>8</sub> O <sub>10</sub> Re <sub>2</sub> S <sub>2</sub>	C <sub>30</sub> H <sub>12</sub> O <sub>20</sub> Re <sub>4</sub> S <sub>2</sub>	C <sub>13</sub> H <sub>8</sub> BrO <sub>5</sub> ReS <sub>2</sub>	C <sub>13</sub> H <sub>9</sub> ClNO <sub>4</sub> ReS <sub>2</sub>	C <sub>18</sub> H <sub>8</sub> O <sub>10</sub> Re <sub>2</sub> S <sub>2</sub>	C <sub>13</sub> H <sub>8</sub> BrO <sub>5</sub> ReS <sub>2</sub>
Formula weight	820.76	1501.32	574.42	528.98	820.76	574.42
Temperature/K	150(2)	150(2)	150(2)	294(2)	150(2)	150(2)
Crystal system	monoclinic	monoclinic	monoclinic	monoclinic	monoclinic	orthorhombic
Space group	P2 <sub>1</sub> /c	P2 <sub>1</sub> /n	P2 <sub>1</sub> /c	P2 <sub>1</sub>	P2 <sub>1</sub> /n	P2 <sub>1</sub> 2 <sub>1</sub> 2 <sub>1</sub>
a/Å	9.6980(5)	10.1212(7)	17.2340(9)	6.5331(8)	9.6861(4)	7.3951(4)
b/Å	13.1478(6)	13.5273(11)	6.4087(4)	11.7969(16)	12.7974(5)	14.2116(10)
c/Å	17.4834(9)	14.1208(12)	16.2660(8)	10.8497(15)	17.8103(8)	15.5998(11)
α/°	90	90	90	90	90	90
β/°	106.099(2)	96.857(4)	116.6180(17)	91.742(5)	104.336(2)	90
γ/°	90	90	90	90	90	90
Volume/Å <sup>3</sup>	2141.84(19)	1919.5(3)	1606.13(15)	835.80(19)	2138.96(16)	1639.48(19)
Z	4	2	4	2	4	4
ρ <sub>calc</sub> /g/cm <sup>3</sup>	2.545	2.598	2.376	2.102	2.549	2.327
μ/mm <sup>-1</sup>	11.542	12.76	10.331	7.692	11.557	10.121
F(000)	1512	1368	1072	500	1512	1072
Crystal size/mm <sup>3</sup>	0.314 × 0.263 × 0.216	0.360 × 0.080 × 0.040	0.194 × 0.169 × 0.163	0.219 × 0.183 × 0.101	0.210 × 0.190 × 0.170	0.380 × 0.260 × 0.220
Radiation	MoKα (λ = 0.71073)	MoKα (λ = 0.71073)	MoKα (λ = 0.71073)	MoKα (λ = 0.71073)	MoKα (λ = 0.71073)	MoKα (λ = 0.71073)
2θ range for data collection/°	4.85 to 63.298	4.696 to 54.198	5.01 to 65.296	5.102 to 54.2	4.398 to 61.014	5.222 to 56.694
Index ranges	-14 ≤ h ≤ 14, -19 ≤ k ≤ 19, -25 ≤ l ≤ 25	-12 ≤ h ≤ 12, -17 ≤ k ≤ 17, -18 ≤ l ≤ 18	-26 ≤ h ≤ 26, -9 ≤ k ≤ 9, -24 ≤ l ≤ 24	-8 ≤ h ≤ 8, -15 ≤ k ≤ 15, -13 ≤ l ≤ 13	-13 ≤ h ≤ 13, -18 ≤ k ≤ 18, -25 ≤ l ≤ 25	-9 ≤ h ≤ 9, -18 ≤ k ≤ 18, -20 ≤ l ≤ 20
Reflections collected	110751	16102	84514	17956	99281	78470
Independent reflections	7210 [R <sub>int</sub> = 0.1020, R <sub>sigma</sub> = 0.0438]	4222 [R <sub>int</sub> = 0.0608, R <sub>sigma</sub> = 0.0412]	5897 [R <sub>int</sub> = 0.0828, R <sub>sigma</sub> = 0.0389]	3683 [R <sub>int</sub> = 0.0725, R <sub>sigma</sub> = 0.0677]	6527 [R <sub>int</sub> = 0.0947, R <sub>sigma</sub> = 0.0368]	4087 [R <sub>int</sub> = 0.0950, R <sub>sigma</sub> = 0.0322]
Data/restraints/parameters	7210/0/291	4222/0/290	5897/0/200	3683/51/224	6527/0/290	4087/12/201
Goodness-of-fit on F <sup>2</sup>	1.061	1.061	1.06	0.94	1.066	1.178
Final R indexes [I>=2σ(I)]	R <sub>1</sub> = 0.0296, wR <sub>2</sub> = 0.0665	R <sub>1</sub> = 0.0303, wR <sub>2</sub> = 0.0563	R <sub>1</sub> = 0.0315, wR <sub>2</sub> = 0.0487	R <sub>1</sub> = 0.0354, wR <sub>2</sub> = 0.0565	R <sub>1</sub> = 0.0247, wR <sub>2</sub> = 0.0497	R <sub>1</sub> = 0.0269, wR <sub>2</sub> = 0.0612
Final R indexes [all data]	R <sub>1</sub> = 0.0432, wR <sub>2</sub> = 0.0713	R <sub>1</sub> = 0.0396, wR <sub>2</sub> = 0.0589	R <sub>1</sub> = 0.0468, wR <sub>2</sub> = 0.0520	R <sub>1</sub> = 0.0574, wR <sub>2</sub> = 0.0623	R <sub>1</sub> = 0.0359, wR <sub>2</sub> = 0.0531	R <sub>1</sub> = 0.0287, wR <sub>2</sub> = 0.0617
Largest diff. peak/hole / e Å <sup>-3</sup>	1.64/-1.99	0.98/-1.43	1.50/-1.73	1.16/-0.61	1.21/-1.88	0.98/-2.15
Flack parameter				0.025(17)		0.406(13)
CCDC No.	1554899	1554895	1554898	1554896	1554900	1554897

**Table S2:** Chemical potential ( $\mu$ ), hardness/MO energy gap ( $\eta$ ) and electrophilicity index ( $\omega$ ) reported in eV for **1a**, **1b**, **3a** and **3b**.

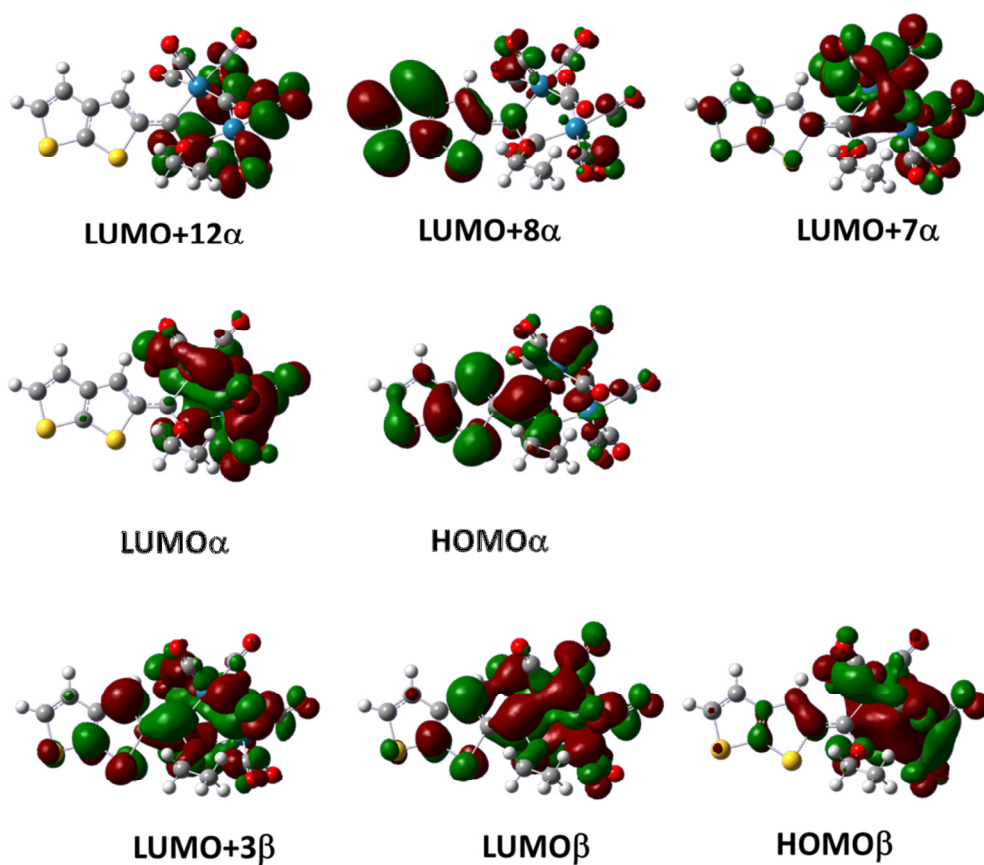
	<b>1a</b>	<b>1b</b>	<b>3a</b>	<b>3b</b>
<b>E<sub>LUMO</sub></b>	-3.3214235	-3.3861866	-3.3616964	-3.4561199
<b>E<sub>HOMO</sub></b>	-6.3603926	-6.3620253	-6.4657008	-6.4363124
<b><math>\mu</math></b>	-4.84090805	-4.87410595	-4.9136986	-4.94621615
<b><math>\eta</math></b>	3.0389691	2.9758387	3.1040044	2.9801925
<b><math>\omega</math></b>	7.7112962	7.983265	7.7784793	8.209219

**Table S3:** Major experimental UV-Vis transitions their corresponding calculated molecular orbitals for **1a**.

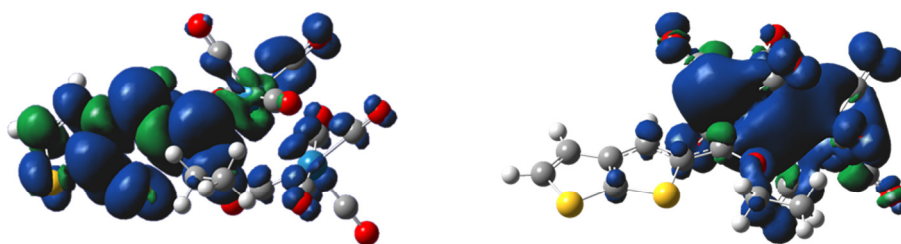
	Major Contributing Excitation (%)	Transition energy (nm)	Oscillator Strength	$\lambda_{\text{exp}}$ (nm)	$\epsilon_{\text{exp}}$ ( $\text{M}^{-1}\text{cm}^{-1}$ )
<b>1a</b>	HOMO $\rightarrow$ LUMO (98)	493	0.223	450	14835
	HOMO-1 $\rightarrow$ LUMO (80) HOMO $\rightarrow$ LUMO+3 (12)	393	0.219	390	12265
	HOMO $\rightarrow$ LUMO+1 (29) HOMO $\rightarrow$ LUMO+3 (49)	341	0.228	320	20995
<b>(1a)<sup>-</sup></b>	HOMO $\alpha$ $\rightarrow$ LUMO+7 $\alpha$ (32) HOMO $\alpha$ $\rightarrow$ LUMO+8 $\alpha$ (51)	538	0.0187	540	315
	HOMO $\alpha$ $\rightarrow$ LUMO+12 $\alpha$ (20), HOMO $\beta$ $\rightarrow$ LUMO $\beta$ (17), HOMO $\beta$ $\rightarrow$ LUMO+3 $\beta$ (19)	403	0.1039	390	6100



**Figure S30:** Normal Transition orbitals (NTOs) for the major absorption bands of **1a**.



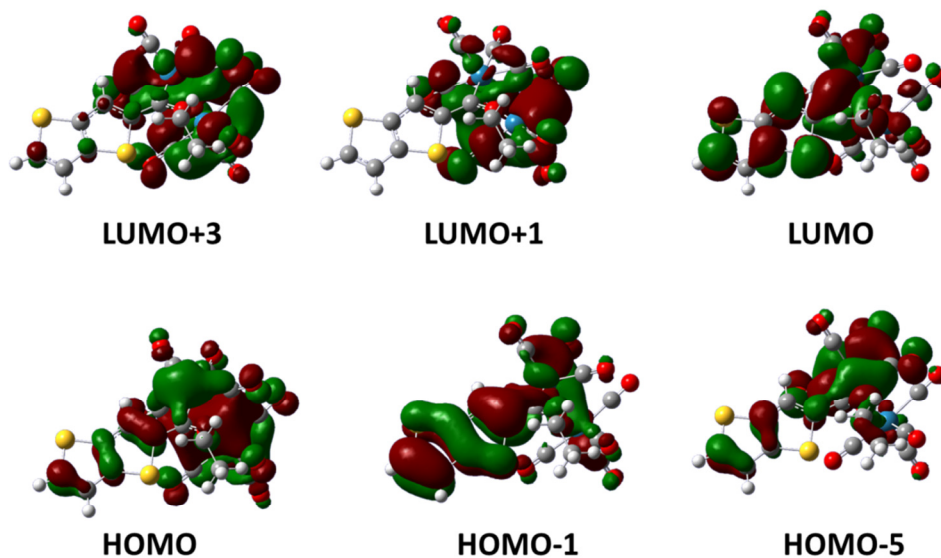
**Figure S31:** Normal Transition orbitals (NTOs) for the major absorption bands of  $1a^-$ .



**Figure S32:** Spin population of  $1a^-$  and  $1a^+$  on the left and right hand side respectively.

**Table S4:** Major experimental UV-Vis transitions their corresponding calculated molecular orbitals for **1b**.

	Major Contributing Excitation (%)	Transition energy (nm)	Oscillator Strength	$\lambda_{\text{exp}}$ (nm)	$\epsilon_{\text{exp}}$ ( $\text{M}^{-1} \text{cm}^{-1}$ )
<b>1b</b>	HOMO→LUMO (99)	497	0.2773	455	14165
	H-1→LUMO (82)	406	0.3036	395	12546
	H-5→LUMO (10) HOMO→L+1 (14) HOMO→L+3 (50)	338	0.1797	322	18907
<b>(1b)<sup>-</sup></b>	HOMO(A) →L+5(A) (57) HOMO(A) →L+8(A) (10) HOMO(A)->L+9(A) (10)	528	0.0126	540	391
	H-1(A) →L+1(A) (14) HOMO(A) →L+8(A) (14) HOMO(B) →LUMO(B) (19) HOMO(B) →L+2(B) (35)	434	0.1213	405	18793

**Figure S33:** Normal Transition orbitals (NTOs) for the major absorption bands of **1b**.

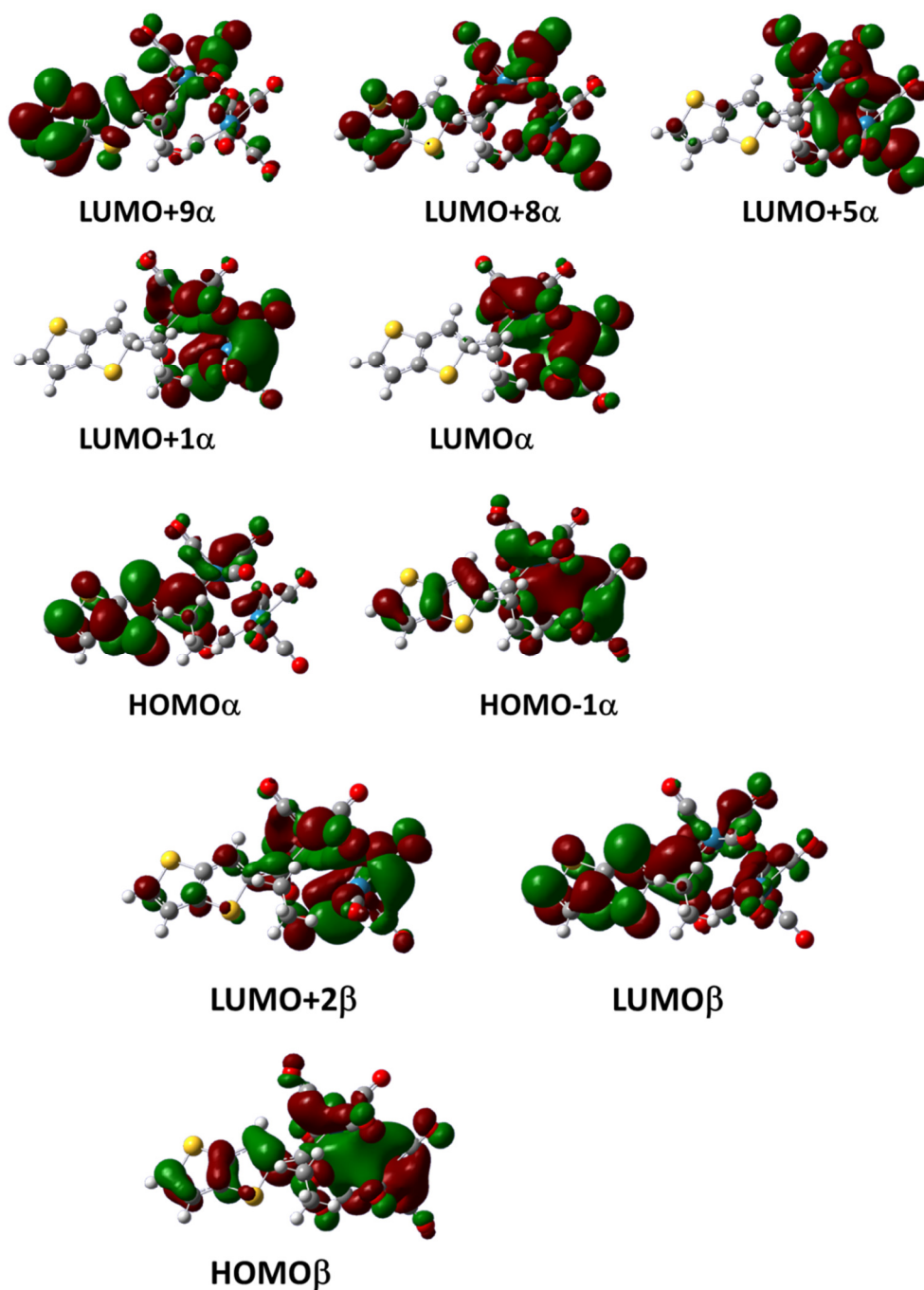


Figure S34: Normal Transition orbitals (NTOs) for the major absorption bands of  $1b^-$ .

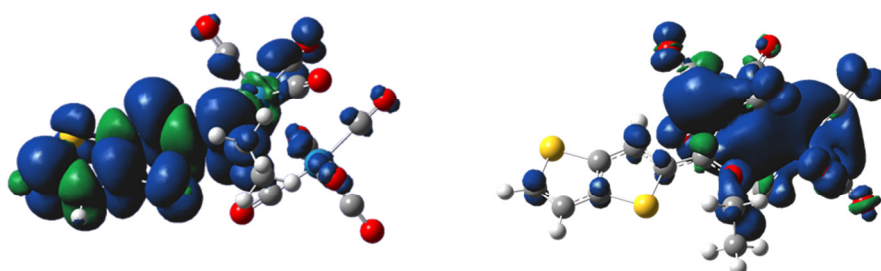
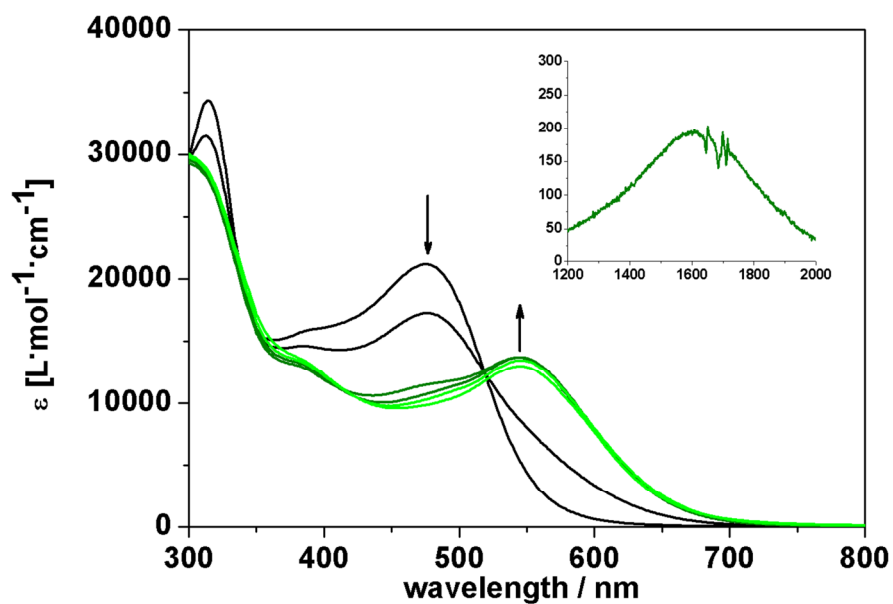
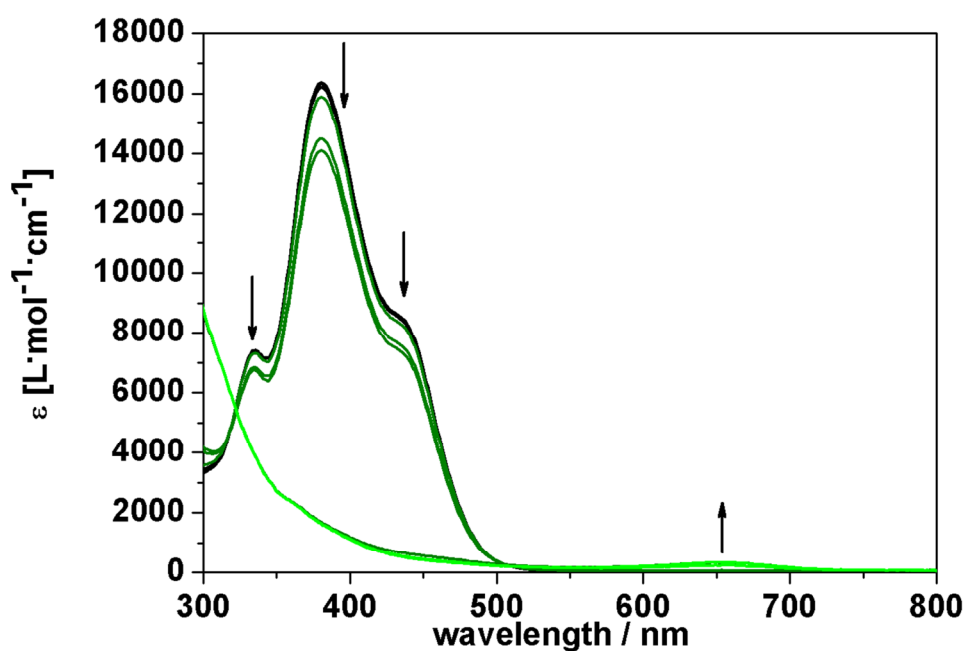


Figure S35: Spin population of  $1b^-$  and  $1b^+$  on the left and right hand side respectively.





**Figure S36:** Changes in UV-Vis absorption spectrum of **2a** during the reduction event in  $\text{CH}_2\text{Cl}_2$  containing 0.1 M  $\text{N}^n\text{Bu}_4[\text{B}(\text{C}_6\text{F}_5)_4]$  electrolyte, applied voltage range: -1.1 to -1.4 V; The inset shows the appearance of a 1600 nm Intervalence charge transfer (IVCT) feature at an applied voltage -1.4 V. (Legend: Increasing cathodic voltages from black to light green)



**Figure S37:** Changes in UV-Vis absorption spectrum of **3a** during the reduction event in  $\text{CH}_2\text{Cl}_2$  containing 0.1 M  $\text{N}^n\text{Bu}_4[\text{B}(\text{C}_6\text{F}_5)_4]$  electrolyte, applied voltage range: -1.1 to -1.4 V (Legend: Increasing cathodic voltages from black to light green)

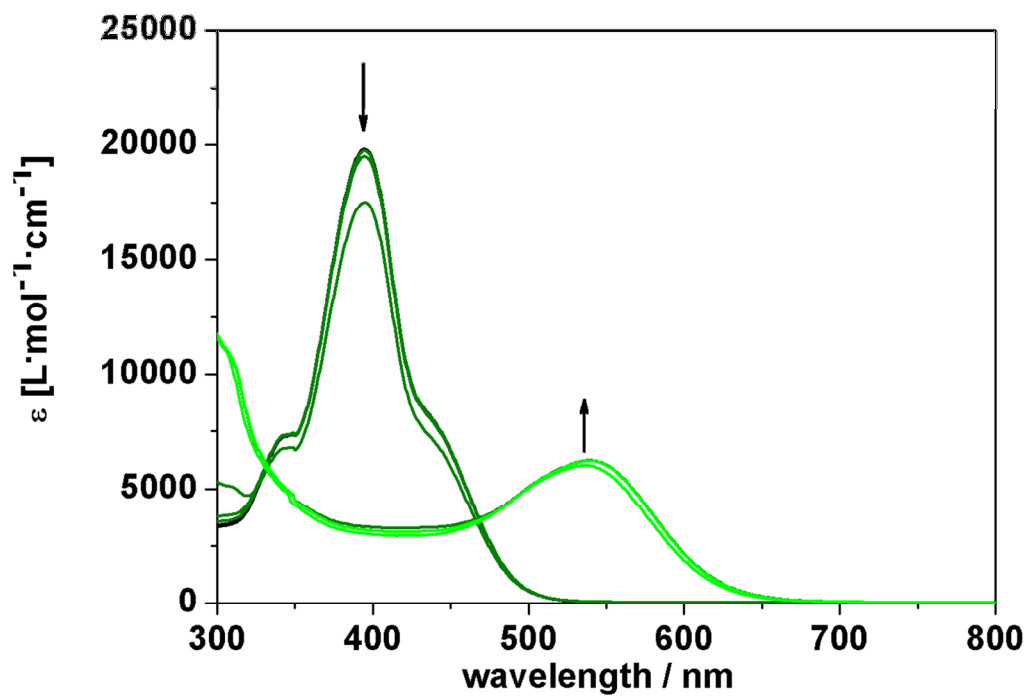


**Figure S38:** Changes in UV-Vis absorption spectrum of **3b** during the reduction event in  $\text{CH}_2\text{Cl}_2$  containing 0.1 M  $\text{N}^n\text{Bu}_4[\text{B}(\text{C}_6\text{F}_5)_4]$  electrolyte, applied voltage range: -1.1 to -1.4 V (Legend: Increasing cathodic voltages from black to light green)